研究成果の刊行に関する一覧表

書籍

著者氏名	論文タイトル名	書籍全体の編集者名	書籍名	出版社名	出版地	出版年	ページ
星美奈子	「かたち」が制御する神経の死：アミロスフェロイドから病態・老化の暗号を解く	小椋光・遠藤遠藤斗志也・森正敬・吉田賢右	「細胞における蛋白質の一生」生成・成熟・輸送・管理・分解・病態	共立出版	東京	2004	1098-1100

雑誌

発表者名	論文タイトル名	発表誌	巻号	ページ	出版年
D. Okada, C.C. Yap, H. Kojima, <u>K. Kikuchi</u> & T. Nagano	Distinct Glutamate Receptors Govern Differential Levels of Nitric Oxide Production in a Layer-specific Manner in the Rat Cerebellar Cortex	*Neuroscience*	**125**	461-472	2004
K. Hanaoka, <u>K. Kikuchi</u>, H. Kojima, Y. Urano & T. Nagano	Development of a Zinc Ion-selective Luminescent Lanthanide Chemosensor for Biological Applications	*J. Am. Chem. Soc.*	**126**	12470-12476	2004
Y. Hu, K.N. Houk, <u>K. Kikuchi</u>, K. Hotta, & D. Hilvert	Nonspecific Medium Effects versus Specific Group Positioning in the Antibody and Albumin Catalysis of the Base-Promoted Ring-Opening Reactions of Benzisoxazoles	*J. Am. Chem. Soc.*	**126**	8197-8205	2004
Asako Kamada, Hisao Nagaya, Taku Tamura, Masataka Kinjo, Hai-Ying Jin, Toshiharu Yamashita1, Kowichi Jimbow, Hideo Kanoh and Ikuo Wada	Regulation of immature protein dynamics in the endoplasmic reticulum	J Biol Chem	**279**	21533-21542	2004
Kenta Saito; Ikuo Wada; Mamoru Tamura and Masataka Kinjo	Direct detection of caspase-3 activation in single live cells by cross-correlation analysis	Biochem. Biophys. Res. Comm	324/2	849-854	2004
<u>K. Kikuchi</u>, K. Komatsu & T. Nagano.	Zinc Sensing for Cellular Applications.	*Curr. Opi. Chem. Biol.,*	**8**	182-191	2004
Lee C.-W., Lee, E.-H., Takeuchi, K., Takahashi, H., Shimada, I., Sato, K., Shin S.-Y.,	Molecular basis of the high-affinity activation of type 1 ryanodine receptors by imperatoxin	A. Biochem. J.,	**., 377**	385-394	2004

Kim, D.-H., and Kim, J.-I					
Manita, S., Kawamura, Y., Sato, K., Inoue, M., Kudo, Y., and Miyakawa., H.:	Adenosine A_1-receptor-mediated tonic inhibition of glutamate release at rat hippocampal Ca3-CA1 synapses in primarily due to inhibition of N-type Ca^{2+} channels.	Eur. J. Pharmacology	**499**	265-274	2004
Nakamura, M., Ishida, Y., Kohno, T., Sato, K., Oba, Y., and Nakamura, H.	Effects of modification at the fifth residue of μ-conotoxin GIIIA with bulky tags in the electrically stimulated contraction of the rat diaphragm.	J. Peptide Res.,	**64**	110-117	2004
Nakai H, Fuess S, Storm T A, Muramatsu S, Nara Y and Kay M A	Unrestricted hepatocyte transduction with AAV serotype 8 vectors in mice	. J Virol	79(1):	214-224	2004
Thwin M.-M., Douni, E., Aidinis, V., Kollias, G., Kodama, K., Sato, K., Satish, R. L., Mahendran, R., and Gopalakrishnakone, P.:	.: Effect of phospholipase A_2 inhibitory peptide on inflammatory arthritis in a TNF transgenic mouse model: a time-course ultrastructural study.	Arthritis Research & Therapy	**6**	282-294	2004
T. Yogo, K. Kikuchi, K. Hirose, M. Iino & T. Nagano	Modification of Intracellular Ca^{2+} Dynamics by Laser Inactivation of Inositol 1,4,5-Trisphosphate Receptor Using Membrane-permeant Probes.	*Chemistry& Biology*	**11**	1053-1058	2004
E. Kawabata, K. Kikuchi, Y. Urano, H. Kojima, A. Odani & T. Nagano	Design and Synthesis of Zinc-Selective Chelators for Extracellular Applications	*J. Am. Chem. Soc*	**127,**	818-819	2005
Sasaki K, Inoue M, Shibata H, Ueda Y, Muramatsu S, Okada T, Hasegawa M, Ozawa K and Hanazono Y	Efficient and stable Sendai virus-mediated gene transfer into primate embryonic stem cells with pluripotency preserved.	Gene Ther,	12(3):	203-210	2004
坂田啓司，藤井文彦，田村　守，金城政孝	「蛍光相関分光法（FCS）を用いた抗原抗体反応解析および検体検出」	バイオインダストリー	4	52-59	2004
村松慎一	パーキンソン病モデルサルへのES細胞由来神経幹細胞の移植	日本再生医療学会雑誌	3	39-44	2004
村松慎一	遺伝子治療. 特集 パーキンソン病	日本臨床	62(9):	1648-1652	2004
星美奈子	新規毒性物質「アミロスフェロイド」の形成と神経細胞死	生化学　総説	76	631-639	2004
星美奈子	新規球状毒性会合体「アミロスフェロイド」の同定-アルツハイマー病発症に置ける神経細胞死機構の解明に向けて	Dementia Japan	18	19-28	2004

星美奈子	βアミロイド自己組織化による神経毒性の発現–新規毒性物質「アミロスフェロイド」とアルツハイマー病	化学と工業	第５７巻、第５号	519-521	2004
星美奈子	神経変性疾患研究の最前線　特集号監修:特集にあたって	Bioindustry	21	5-7	2004
星美奈子	アミロスフェロイド-タンパク質の自己組織化と神経変性疾患	Bioindustry	21	67-74	2004
星美奈子	球状βアミロイド凝集体アミロスフェロイドー蛋白質の自己組織化と神経細胞死	Cognition and Dementia	3	359-366	2004

IV．研究成果の刊行物・別刷り

DISTINCT GLUTAMATE RECEPTORS GOVERN DIFFERENTIAL LEVELS OF NITRIC OXIDE PRODUCTION IN A LAYER-SPECIFIC MANNER IN THE RAT CEREBELLAR CORTEX

D. OKADA,[a,b,c*] C. C. YAP,[a] H. KOJIMA,[d] K. KIKUCHI[d]
AND T. NAGANO[d]

[a]*Laboratories for Memory and Learning, and Cellular Information Processing, Brain Science Institute, RIKEN, Wako, Saitama 351-0198, Japan*

[b]*Precursory Research for Embryonic Science and Technology, JST, Kawaguchi, Saitama 332-0012, Japan*

[c]*Brain Science and Life Technology Research Foundation, Itabashi, Tokyo 175-0094, Japan*

[d]*Graduate School of Pharmaceutical Sciences, University of Tokyo, Bunkyo, Tokyo 113-0033, Japan*

Abstract—To evaluate roles of nitric oxide (NO) in neural functions, it is critical to know how neural inputs activate neuronal NO synthase in individual sites. Although NMDA receptor-dependent mechanism well explains postsynaptic, robust NO production, this sole mechanism does not explain some aspects of NO production in the brain, such as the low-level production of NO and the mechanism for presynaptic NO production. We hypothesized that the glutamate receptor involved in NO production is site-specific and controls the initial NO concentration in each site. We visualized NO production mediated by NMDA, AMPA and type-1 metabotropic glutamate (mGlu-1) receptors in rat cerebellar slices and granule cells in culture, with an NO-specific fluorescent indicator, diaminofluorescein-2. AMPA receptor, but not NMDA or mGlu-1 receptor, was responsible for NO production at parallel fiber terminals, which was blocked by CNQX, tetrodotoxin or voltage-dependent calcium channel blockers. More numbers of electrical stimulation were required for NO production in the molecular layer than in other layers, suggesting that AMPA receptor activation generates NO at lower concentrations through a remote interaction with NO synthase. Although Purkinje cell does not express NO synthase, we detected NO production in Purkinje cell layer following electrical stimulation in the white matter at 50 Hz, but not at 10 Hz. This NO production was tetrodotoxin-sensitive, suggesting occurrence in the basket cell terminals, and required

Correspondence to: D. Okada, Mitsubishi Kagaku Institute of Life Sciences (MITILS), 11 Minami-Ooya, Machida, Tokyo 194-8511, Japan. Tel: +81-42-724-6257; fax: +81-42-724-6257.
E-mail address: dada@libra.ls.m-kagaku.co.jp (D. Okada).
Abbreviations: ACSF, artificial cerebrospinal fluid; CNQX, 6-cyano-7-nitroquinoxaline-2,3-dione disodium salt; CPCCOEt, 7-(hydroxy-imino)-cyclopropa-[b]-chromen-1a-carboxylate ethyl ester; DAF-2, diaminofluorescein-2; D-AP5, D-2-amino-5-phosphonovaleric acid; DAR-4M, diaminorhodamine-4M; DIV, days *in vitro*; DTCS, *N*-(dithiocarboxy)-sarcosine; GC, granule cell; GCL, granule cell layer; L-NAME, *N*$^\omega$-nitro-L-arginine methyl ester; mGlu-1, type-1 metabotropic glutamate; ML, molecular layer; nNOS, neuronal nitric oxide synthase; NO, nitric oxide; PC, Purkinje cell; PCL, Purkinje cell layer; PF, parallel fiber; ROI, region of interest; (S)-DHPG, (S)-3,5-dihydroxyphenylglycine; TMA-DPH, 1-(4-trimethylammonium-phenyl)-6-phenyl-1,3,5-hexatriene-*p*-toluene sulfonate; TTX, tetrodotoxin; WM, white matter.

synergistic activation of mGlu-1 and NMDA receptors. In the granule cell layer, activation of AMPA or mGlu-1 receptor produced NO uniformly, while NMDA receptor activation produced NO in discontinuous areas of this layer. Thus, distinct glutamate receptors, including non-NMDA receptors, govern occurrence and level of NO production in a layer-specific manner. © 2004 IBRO. Published by Elsevier Ltd. All rights reserved.

Key words: AMPA receptor, NMDA receptor, mGlu-1 receptor, DAF-2, parallel fiber.

Nitric oxide (NO) serves as an intercellular signal involved in synaptic plasticity (Shibuki and Okada, 1991; Boehme et al., 1991; Calabresi et al., 1999), activity-dependent synapse formation (Wu et al., 1994) and neuronal development (Tanaka et al., 1994). To evaluate roles of NO in these neural functions, it is critical to know how neural inputs activate neuronal NO synthase (nNOS) in individual sites. It is widely accepted that NMDA receptor activation triggers production of NO at near-maximal rate due to the close linkage between the NMDA receptor and nNOS by PSD-95 (Brenman et al., 1996; Christopherson et al., 1999). This coupling seems to be central for glutamatergic activation of nNOS. However, there are many aspects in neuronal NO production that are not readily explained solely by the NMDA receptor-dependent mechanism.

The first aspect is related to NO concentrations generated by nNOS. Malinski and Taha (1992) measured bradykinin-dependent NO production from cultured endothelial cells with their electrochemical probe, and detected 450 nM NO. The responsible NOS, eNOS, has Vmax about 10 times lower than that of nNOS (Förstermann and Gäth, 1996); therefore it is deduced that the nNOS maximal activation causes production of 4.5 µM NO. On the other hand, direct electrochemical measurements showed that parallel fiber (PF) stimulation produced NO only at 5 nM in the molecular layer (ML) of cerebellar slices (Shibuki and Kimura, 1997). This discrepancy suggests a possibility that input activity does not necessarily evoke full activation of NOS. However, it is not clear how low level activation of NOS is achieved by neuronal activity.

Second, it is known that the initial NO concentrations determine the diffusion range of NO, which is a critical factor for NO action in brain tissues, an assembly of neurons with heterogeneous activity states (Gally et al., 1990; Wood and Garthwaite, 1994). NO from one potent source may affect cells located outside of the activated neuronal circuit. Such an information leakage outside of the 'wired

circuit' reduces spatial specificity of information transfer. However, this leakage may have physiological influence on the circuit behavior such as contrast formation (Krekelberg and Taylor, 1996) or distributed synaptic plasticity (Schuman and Madison, 1994; Hartell, 1996). For this purpose, it is expected that the initial NO concentrations, thereby the spreading areas, are tunable, or graded in response to synaptic inputs. Actually, the NO production rate in ML depended on stimulus frequency and cyclic AMP-dependent protein kinase (Shibuki and Kimura, 1997; Kimura et al., 1998). However, the NMDA receptor mechanism is not suitable to control the graded NO production. Actually, the only variation of NO production through NMDA receptor is pathological, in which prolonged activation of the receptor causes neuronal death (Sattler et al., 1999).

Finally, nNOS immunoreactivities in the cerebellar cortex were found both presynaptically (terminals of PF and basket cell axon called the pinceau) and postsynaptically (dendrites of basket/stellate and granule cells [GC]; Rodrigo et al., 1994). Although it is well known that NMDA receptor is the major trigger of NO production in the postsynaptic sites (Garthwaite et al., 1988; Bredt and Snyder, 1990), mechanism for presynaptic NO production is yet unclear. For example, there is a controversy as to the responsible receptor for NO production in PF terminals (Shibuki and Kimura, 1997; Casado et al., 2000; Hartell et al., 2001). In addition, NO production has not yet been described in the pinceau.

Pharmacological studies revealed that activation of AMPA or type-1 metabotropic glutamate (mGlu-1) receptor also produced NO in the cerebellar slices (Okada, 1992), although contributions of these receptors in total cyclic GMP formation were relatively small (Bredt and Snyder, 1989). These facts and considerations suggested a hypothesis that multiple receptor mechanisms control the efficiency of NO production at specific sites, allowing variation in NO functions. In the present study, we visualized NO production in rat cerebellar cortex by the use of a NO-specific fluorescence indicator dye, diaminofluorescein-2 (DAF-2; Kojima et al., 1998), and found that distinct receptor mechanisms governed NO production in presynaptic sites. AMPA receptor activation produced NO at low concentrations in PF terminals, while synergistic activation of NMDA and mGlu-1 receptors produced NO around Purkinje cell (PC) soma, probably in the pinceau.

EXPERIMENTAL PROCEDURES

Cerebellar slices and culture

Wistar ST rats (7–10 weeks old; Japan SLC, Japan) were decapitated under ether anesthesia, according to RIKEN's guideline of the animal care and use. All efforts were made to minimize the number of animals used and their suffering. Cerebellar vermal slices (usually 300 μm thick and 150 μm in Fig. 2) were prepared with a vibrating slicer (Dosaka EM, Japan) as described (Okada, 2000) in ice-cooled artificial cerebrospinal fluid (ACSF), which contained (mM): NaCl 125, KCl 2.5, $CaCl_2$ 2, $MgCl_2$ 1, NaH_2PO_4 1.25, $NaHCO_3$ 26, glucose 25, and was bubbled with 95% O_2 and 5% CO_2 (pH 7.4). Primary neuronal culture was prepared from E19-20 Wistar ST rat cerebella

by the method of Furuya et al. (1998). After digestion with 0.1% trypsin and 0.05% DNAse A at 37 °C, cell suspensions were incubated on a poly-L-ornithine-coated (10 μg/ml) dish at 37 °C for 20 min, then cells not attached to the dish were seeded at 2×10^5 cells/well on poly-L-ornithine-coated (250 μg/ml) plastic sheets (12 mm diameter; Sumilon; Sumitomo Co. Ltd.), and cultured in six-well plates. Ara-C (1 μM) was added to the medium 2–8 days in vitro (DIV). Under this condition, about 70% of the cell population was constituted with GCs.

Imaging

Slices or cells on DIV 14–21 were incubated with 10 μM DAF-2 diacetate at 32 °C for 30 min in dark. In some experiments cells were incubated with diaminorhodamine-4M (DAR-4M) AM (10 μM, 30 min) and 1-(4-trimethyl ammoniumphenyl)-6-phenyl-1,3,5-hexatriene-p-toluenesulfonate (TMA-DPH; 20 μM; 1 min) at 37 °C (Bronner et al., 1986). To incorporate TMA-DPH into recycling vesicles, cells were stimulated with AMPA for 1 min, washed with ACSF for 60 min, and then stimulated by 90 mM KCl for 2 min at room temperature. Fluorescence representing recycling vesicles appeared in subtraction images (before minus after KCl).

Slices, under constant perfusion with ACSF (1.5 ml/min) maintained at 32 °C using an inline heater (TC344B; Warner, USA), were observed with an upright fluorescence microscope (BX50-WI; Olympus) equipped with a 150 W xenon lamp and an electric shutter (OSP-EXA; Olympus). A platinum weight and a nylon net were used to prevent slice movements. Cultures under constant perfusion with ACSF (0.7 ml/min) at room temperature were observed with an inverted fluorescence microscope (Axiovert S100-25; Zeiss) equipped with a 100 W mercury lamp and an electric shutter (Uniblitz D122; Vincent Associates, USA). Fluorescent images (12 bit, 512×512 pixels) of DAF-2 (exciter 470–490 nm, dichroic mirror 500 nm, emitter >505 nm), DAR-4M (530–560 nm, 570 nm, >605 nm) and TMA-DPH (380–400 nm, 405 nm, 410–460 nm) were acquired with a cooled CCD camera (PXL37; Photometrics, USA). Exposure (50–300 ms) and image acquisition were controlled by an electric stimulator (Master-8; AMPI, Israel). Images were stored in a personal computer (Power Macintosh 9500/200) and analyzed off-line with IPLab software (Scanalytics, USA).

Stimulation

Drugs were applied by switching the medium with a six-way valve (type 50; Rheodyne). Complete exchange of the medium in the chamber took 1 min under the flow rate at 1.5 ml/min, judged from measurement of chloride potential shift. AMPA (1–50 μM, usually 10 μM) and (S)-3,5-dihydroxyphenylglycine ((S)-DHPG; 100 μM) were applied for 1 and 5 min, respectively. NMDA (30 μM; in some experiments 100 μM) was dissolved in Mg^{2+}-free ACSF containing 10 μM glycine, and applied for 1 min, which was always preceded by application of Mg^{2+}-free ACSF for 15 min. Electrical stimulation (a SEN7203 stimulator and a SS201J isolator; Nihon Kohden, Japan) was given through a tungsten bipolar electrode (WPI; tip resistance 2 MΩ) positioned 150 μm beneath the slice surface. PF presynaptic volleys were recorded (Axopatch 200B; Axon Instruments, USA) with extracellular glass pipettes (5 MΩ) placed on the surface of frontal slices 500 μm apart from the stimulating site (Casado et al., 2000).

Analysis

To find a region of interest (ROI), a subtraction image (response peak minus pre-stimulus average) was made and its pixel intensity histogram was calculated. A ROI was selected among pixels showing changes larger than a half of the maximum change in the histogram. Intensity histogram of an eight-bit image was calculated and pseudocolors were applied (Okada, 2000). Membrane densities affect incorporation of hydrophobic DAF-2 diacetate,
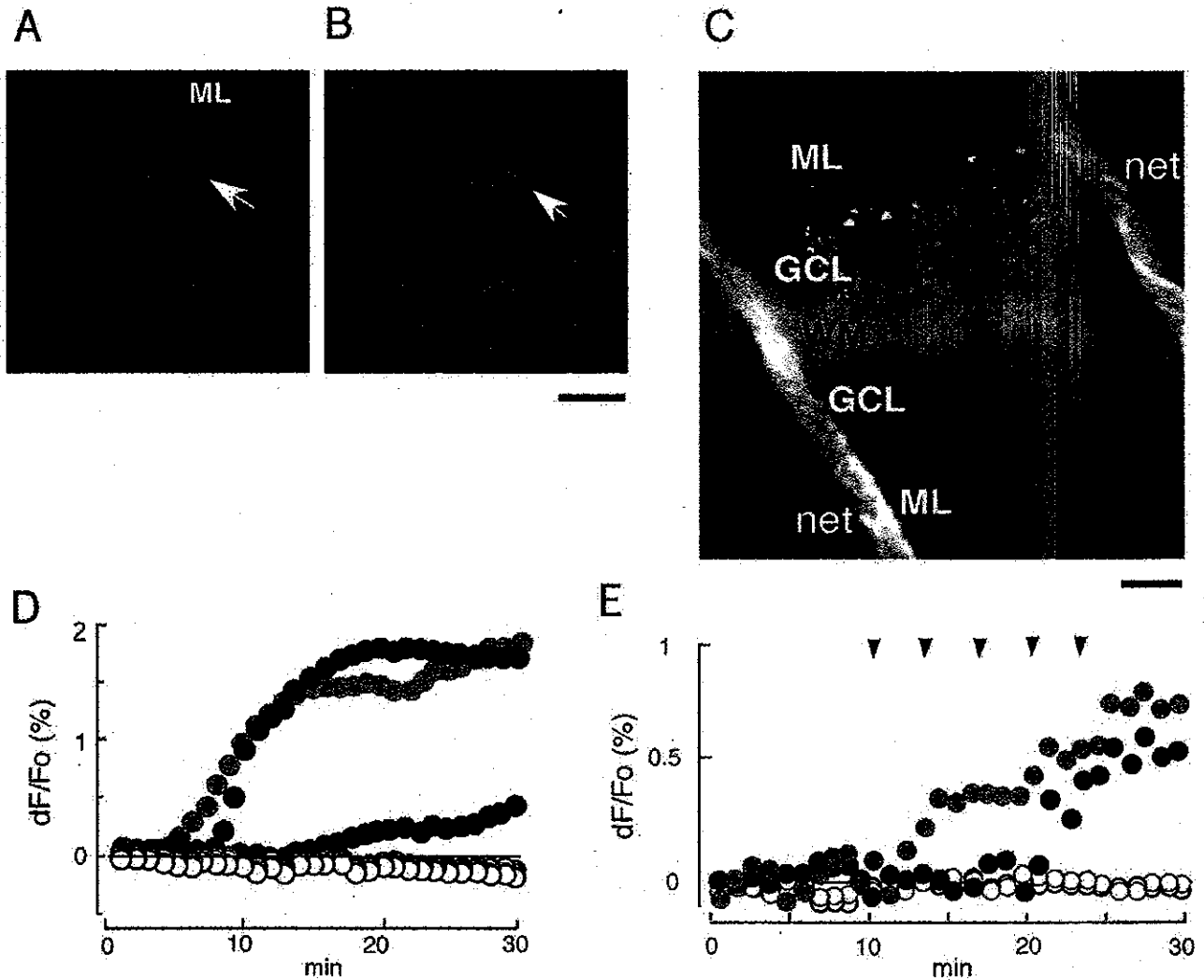
A

B

C

D

E

Fig. 1. NO production evoked by electrical stimulation suggests layer-dependent mechanisms. (A–D) Ten trains (0.5 Hz) of 20 biphasic pulses (duration: 0.1 ms; amplitude: ±0.5 V; frequency: 20 Hz) were given to the WM of a sagittal slice every minute. (A) A fluorescence image (×40 objective) before stimulation. Fluorescence in ML was low, while individual GCs are more fluorescent. A PC soma indicated by an arrow was weakly fluorescent. (B) The same site as in A after 30 sets of stimulation (i.e. 30 min after A). Dendrites and soma of a PC indicated by an arrow and GCs are now intensely fluorescent. Scale bar=50 μm. (C) A low magnitude (×5) image of B. Position of stimulation is indicated by a X. The nylon net preventing movement of slice is seen (net). Scale bar=100 μm. (D) Fluorescence changes in ROIs shown by squares in C were measured and normalized in the initial intensity (dF/Fo). A representative experiment from six similar experiments is shown by closed symbols. Green, GC; red, PC soma; blue, ML. Similar experiments were done in the presence of 10 μM L-NAME (open symbols). A representative experiment from three similar experiments is shown. (E) ML of a frontal slice was stimulated with five trains (0.5 Hz) of 50 biphasic pulses (duration: 1 ms; amplitude: ±30 V; frequency: 50 Hz) at time points indicated by arrowheads. A representative experiment from three similar experiments is shown by closed symbols. Green, GCL; blue, ML. Similar experiments were done in the presence of 10 μM L-NAME (open symbols). A representative experiment from three similar experiments is shown.

thus intracellular DAF-2 concentrations. Actually, GC layer (GCL) showing granular patterns of intense fluorescence was easily discriminated from ML where almost even staining was observed. Comparison of the fluorescence increase between different layers therefore requires normalization by the initial fluorescence intensity (dF/Fo), while fluorescence time courses within one ROI can be expressed by fluorescence increase (dF).

Materials and other methods

DAF-2 diacetate (Kojima et al., 1998) and DAR-4M AM (Kojima et al., 2001) were synthesized as reported, or supplied from Daiichi

Pure Chemicals Co. Ltd. (Japan). NMDA (Nakalai Tesque, Japan), (S)-AMPA, (S)-DHPG, 7-(hydroxyimino)-cyclo propa-[b]-chromen-1a-carboxylate ethyl ester (CPCCOEt), 6-cyano-7-nitro quinoxaline-2,3-dione disodium salt (CNQX), D-2-amino-5-phosphonovaleric acid (D-AP5), N^ω-nitro-L-arginine methyl ester (L-NAME; Tocris Cookson, UK), N-(dithiocarboxy)-sarcosine (DTCS; Dojindo, Japan), ω-conotoxin-GIVA, ω-agatoxin-TK, nifedipine (Alamone Laboratory, Israel), TMA-DPH (Molecular Probe, USA) and tetrodotoxin (TTX; Seikagaku Kougyo, Japan) were purchased. Cyclic GMP was measured using an enzyme-linked immuno assay kit (Amersham Pharmacia, UK) as reported (Miyata et al., 1999).
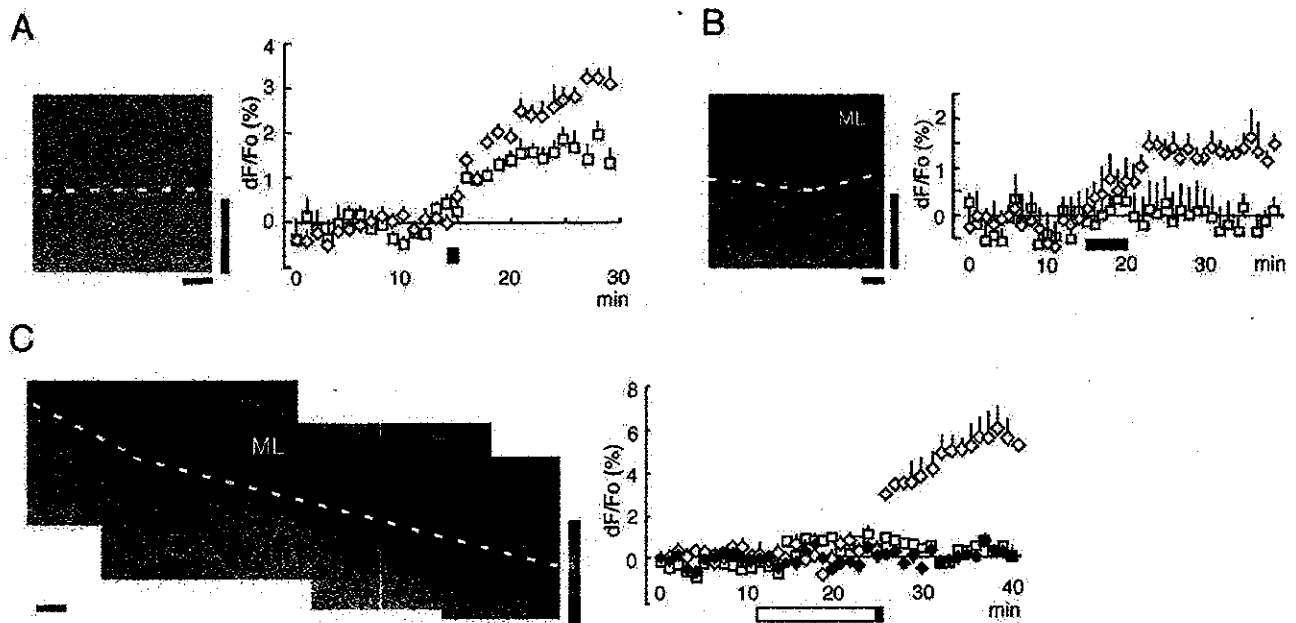
Fig. 2. Differential NO production by type-specific glutamate receptor agonists. (A, B) A receptor type-specific agonist was applied to thin (150 μm thick) horizontal slices. (Left) A subtraction image (20 min after stimulation–before, ×20 objective). Broken lines indicate PCL. Scale bar=20 μm. (Right) The time course of average dF/Fo in five ROIs (squares, ML; diamonds, GCL) are shown. Vertical bars are S.E.M. Horizontal bars represents application of 10 μM AMPA (A) and 100 μM (S)-DHPG (B). (C, Left) Fluorescence images (×10) were taken in adjacent regions in the lobule VI before and after 30 μM NMDA application. Images were aligned and subtraction images were calculated, equal pseudocolors were applied to corresponding loci, and merged. Regions with intense fluorescence increase appeared discontinuously as indicated by arrowheads. (Right) Averages of dF/Fo in five ROIs are shown over time. Open and closed bars indicate application of Mg-free ACSF and NMDA, respectively. Open diamonds, GCL with increase; closed diamonds, GCL without increase; squares, ML. Scale bar=100 μm.

RESULTS

Entire picture of NO production in the cerebellar cortex

Fig. 1A shows an example of DAF-2 fluorescence in a parasagittal slice before stimulation. Weak fluorescence was found uniformly in neurons, consistent with the amphipathic nature of the DAF-2 (DAR-4M as well) molecule. Incorporation in glia was not evident. Perfusion with ACSF alone did not alter the fluorescence for at least 1 h. To know the entire sites of NO production in the cerebellar cortex, electrical stimulation was given repeatedly to the white matter (WM) of parasagittal slices ($n=6$). Fig. 1B and C shows that GCs, PCs and ML were intensely fluorescent. Although PCs do not express nNOS (Crepel et al., 1994), a whole PC was fluorescent, indicating that the PC received NO derived from surrounding sources, consistent with our previous observations (Hartell et al., 2001). As seen in Fig. 1C, a restricted region of a folium responded, showing that our stimulation activated specific neural circuits. Fig. 1D (closed symbols) shows an example of experiments ($n=3$) where a NOS inhibitor, L-NAME at 10 μM, blocked the increase, confirming the fluorescence change was due to NO production. We confirmed the blockade by L-NAME of the fluorescence change for all types of electrical or agonist stimulation in this study (see Discussion).

Fig. 1D also shows that onset and magnitude of fluorescence increase differed in each layer: fluorescence increase in ML was much lower and required more numbers of stimulation than the other layers. Although the onset

delays somewhat differed among experiments, this tendency was constantly observed. Such a delayed onset may reflect attenuation of conduction between distant sites (from WM to ML), or it may reflect the fact that most of PFs are cut in parasagittal slices. Alternatively, single stimulation may produce different concentrations of NO in each layer. To clarify this issue, ML of frontal slices, where PFs are preserved, was stimulated repeatedly. Since the stimulation parameters used in sagittal slices did not alter fluorescence in GCs of frontal slices, stronger stimulation parameters were applied to activate GCs retrogradely. This stronger stimulation successfully increased fluorescence in both layers. As shown in Fig. 1E, the fluorescence increase in ML, which was inhibited by L-NAME, also required more numbers of stimulation than in GCL ($n=3$): GCL and ML required one to two and three to four trains of stimulation, respectively. Thus, the delayed onset was independent of stimulation sites or direction of slice sectioning. These results are consistent with the idea that NO production rate in ML is lower than in the other area.

Localization of NO production by specific receptor activation

Results shown in Fig. 1 were consistent with the hypothesis that each layer employs different NO producing mechanisms. Pharmacological stimulation of each receptor further supported this idea. Application of 1–50 μM AMPA increased fluorescence in ML of horizontal ($n=4$; Fig. 2A), parasagittal ($n=3$; see Fig. 6A) and frontal slices ($n=3$; not shown). In contrast, a specific agonist of mGlu-1 receptor,
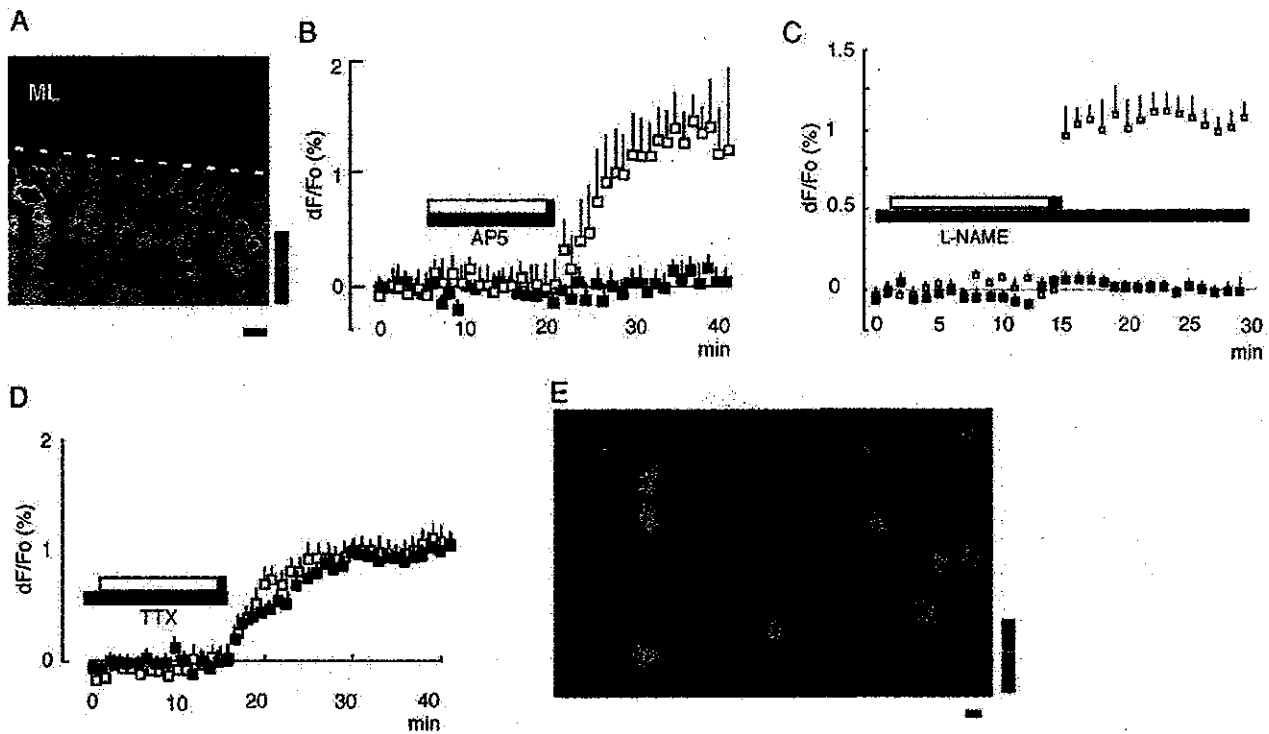
Fig. 3. NMDA receptor-dependent NO production. (A) A subtraction image (×40) showing response of a parasagittal slice to 30 μM NMDA. Broken line indicates PCL. Note that response was seen only in GCL. (B–D) Fluorescence increases evoked by NMDA (open symbols) in GCL of parasagittal slices were inhibited by 50 μM D-AP5 (red symbols; four ROIs from three slices; B) and 10 μM L-NAME (green symbols; 10 ROIs from five slices; C), but not by 1 μM TTX (blue symbols; 10 ROIs from three slices; D). Antagonists, Mg-free ACSF and NMDA were applied during periods indicated by colored, open and black bars, respectively. Averages and S.E.M. (vertical bars) of dF/Fo are shown. (E) A subtraction image (×40 objective) depicting NMDA-dependent fluorescence increase in soma of GCs in culture on DIV 15. Scale bars in A and E=20 μm and 10 μm, respectively.

(S)-DHPG (100 μM; horizontal slices, n=4, Fig. 2B; parasagittal slices, n=5, not shown), or NMDA (30 μM; horizontal slices, n=3, Fig. 2C; parasagittal, n=5, see Fig. 3A; frontal, n=3, not shown) did not alter it. These results depicted the major contribution of AMPA receptor to NO production in ML, while contributions of NMDA and mGlu-1 receptors were under the detection level.

In contrast, DAF-2T fluorescence in GCL was increased by all of the agonists used. AMPA (Fig. 2A) or (S)-DHPG (Fig. 2B) increased fluorescence uniformly in the entire GCL. However, NMDA application resulted in fluorescence increase in discontinuous areas in GCL of thin (150 μm thick) horizontal slices (folium VI, n=3, Fig. 2C). We could not detect such a discontinuous pattern in frontal and sagittal slices.

NMDA receptor mechanisms

NMDA application to sagittal slices specifically increased fluorescence in GCL (Fig. 3A), which was blocked by D-AP5 (n=3, Fig. 3B) or L-NAME (n=5, Fig. 3C), indicating that NMDA receptor-dependent NOS activation takes place in GCL. A close linkage between NMDA receptor-mediated calcium influx and nNOS activation (Christopher-son et al., 1999) suggests that NMDA triggers NO production without conduction of depolarization in the absence of extracellular Mg^{2+} ions. This idea was confirmed by experiments shown in Fig. 3D, where TTX did not affect

NMDA-dependent NO production in GCL (n=3). When NMDA was applied to GCs in dissociated culture, fluorescence was increased predominantly in the soma, and the proximal neurites to a less extent, but not in the fine, distal neurites (n=5, Fig. 3E), suggesting postsynaptic localization of the mechanism.

AMPA receptor mechanisms

When frontal slices were received electric stimulation (parameters identical to that used in Fig. 1E) in ML, an AMPA receptor antagonist, CNQX, blocked the fluorescence increase in ML (n=4, Fig. 4), while a NMDA receptor antagonist, D-AP5, had no significant effect (n=4, Fig. 4). These results were consistent with results shown in Fig. 2, confirming the major contribution of AMPA receptors in NO production in ML. Fluorescence increases in ML and GCL evoked by bath-applied AMPA were also inhibited by CNQX (n=4, Fig. 5A), or L-NAME (n=4, Fig. 5B), but not by D-AP5 (n=2, Fig. 5A). These results confirmed that AMPA receptor, but not NMDA receptor, triggered NOS activation. In contrast to NMDA, TTX reduced the AMPA-dependent NO production in both ML and GCL (n=6, Fig. 5C), suggesting that AMPA receptor and NOS are indirectly linked through conduction of depolarization. AMPA also increased fluorescence of GCs in culture (Fig. 5D), which was similarly inhibited by CNQX (n=4), L-NAME (n=4) or TTX (n=3) (data not shown). In both slices (ML and GCL) and culture, a blocker of N-type calcium
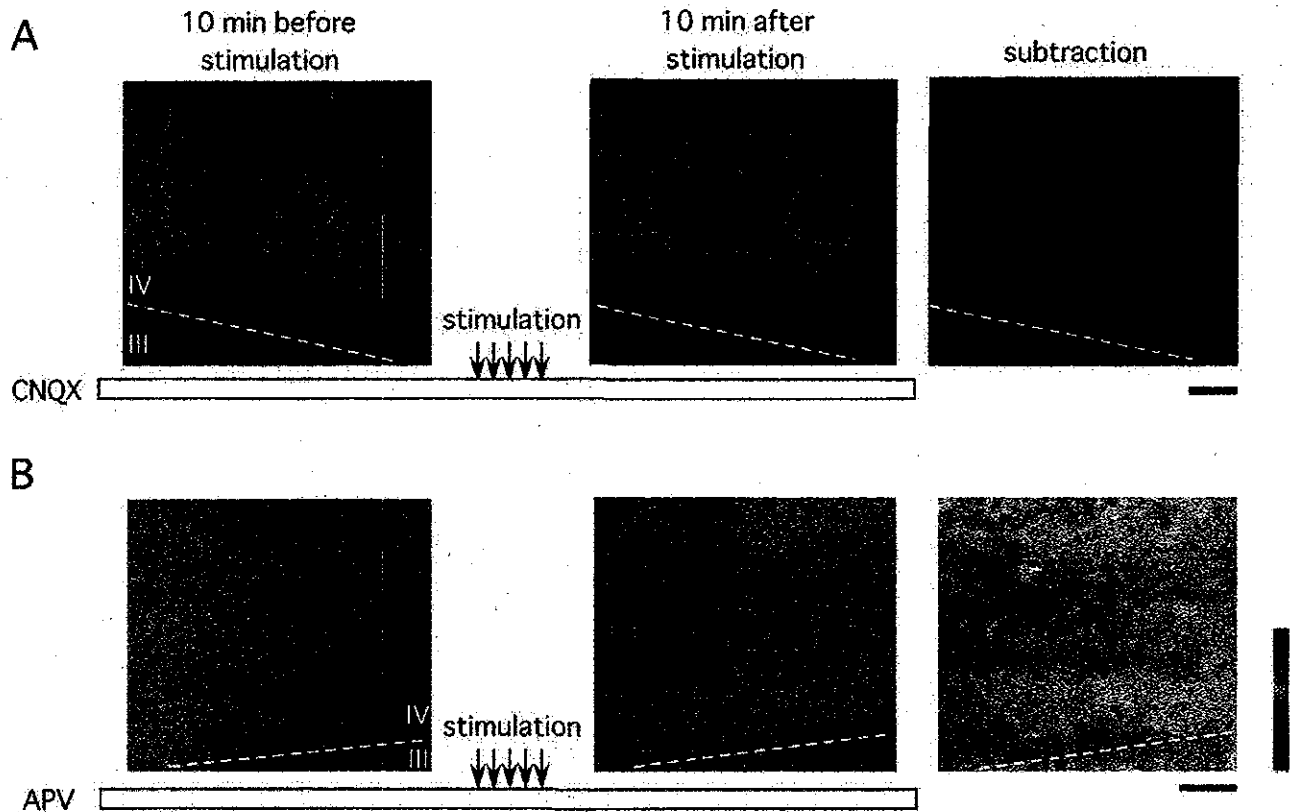
Fig. 4. AMPA receptor is responsible for NO production in ML. ML of a frontal slice was electrically stimulated (50 biphasic pulses with 1 ms of duration and ±30 V of amplitude at 50 Hz, five trains every 2 s, shown by arrows). CNQX (50 μM) abolished fluorescence change in ML (A), while D-AP5 (50 μM) did not suppress it (B). (Left and Center) Raw fluorescence images of ML before and after stimulation are shown in pseudocolors. (Right) A peristimulus subtraction image. Broken lines indicate the border of folia III and IV. Scale bars=20 μm.

channel, ω-conotoxin-GIVA (1 μM, 10 min, $n=3$ for each, Fig. 5E), or P/Q-type calcium channel, ω-agatoxin-TK (0.1 μM, 10 min, $n=3$ for each, Fig. 5F), abolished AMPA-dependent fluorescence increase, whereas the L-type channel blocker, nifedipine had no effect (10 μM, 10 min, $n=3$ for each, Fig. 5G). These results are consistent with the previous reports (Okada, 1992; Shibuki and Kimura, 1997) and demonstrated that calcium influx in compartments linked to N- and P/Q-type calcium channels activate NOS after conduction of depolarization triggered by AMPA receptor activation.

Although AMPA produced NO in the entire ML relatively uniformly in horizontal (Fig. 2A) and frontal slices, the response was not uniform in parasagittal slices (Fig. 6A) where only a small portion of PFs is connected with the originating GCs. As shown in Fig. 6A, regions with larger increases were recognized as fluorescent patches. Line-scan analysis of such a patch (Fig. 6B) showed that NO was generated from small sources, because the increase started from single pixels. These single fluorescent pixels were then merged to shape the fluorescence patch (about 5 μm of radius).

Immunohistochemical studies (Rodrigo et al., 1994) showed that PF terminals and interneurons are possible NO sources in ML. To distinguish these possibilities we noticed difference in their size. A water-soluble NO scavenger, Fe-DTCS (Fujii et al., 1998), that traps extracellular

NO, was used to highlight single components of the source by scavenging intercellularly spreading NO. If PF terminals are the source, the patches should disappear in the presence of the scavenger, because single components (=terminal) are very small (<1 μm) compared with the patch (10 μm). Alternatively, if interneurons are the source, NO spreading inside the cell will not be wiped out by the scavenger; therefore, as a result interneuron should be highlighted. Because the diameter of the single components (=interneuron soma) is similar to that of the patch, they should not disappear, but even be highlighted, in the presence of scavenger. Results showed that Fe-DTCS eliminated the patches ($n=3$, Fig. 6C), suggesting that intercellular diffusion of NO from PF terminals shaped the patch. NO release from PF terminals was directly detected GCs in culture, where AMPA increased DAF-2 fluorescence in fine fibers, as well as in soma (Fig. 6D). To confirm NO production at PF terminals, recognized as axonal varicosities, GCs in culture were doubly stained with DAR-4M, another NO-specific indicator with red fluorescence (Kojima et al., 2001), and TMA-DPH, an activity-dependent endocytosis marker with blue fluorescence (Bronner et al., 1986). This dual staining enabled simultaneous observation of NO production and activity-dependent endocytosis that occurs predominantly in presynaptic terminals. The result indicated colocalization of endocyto-
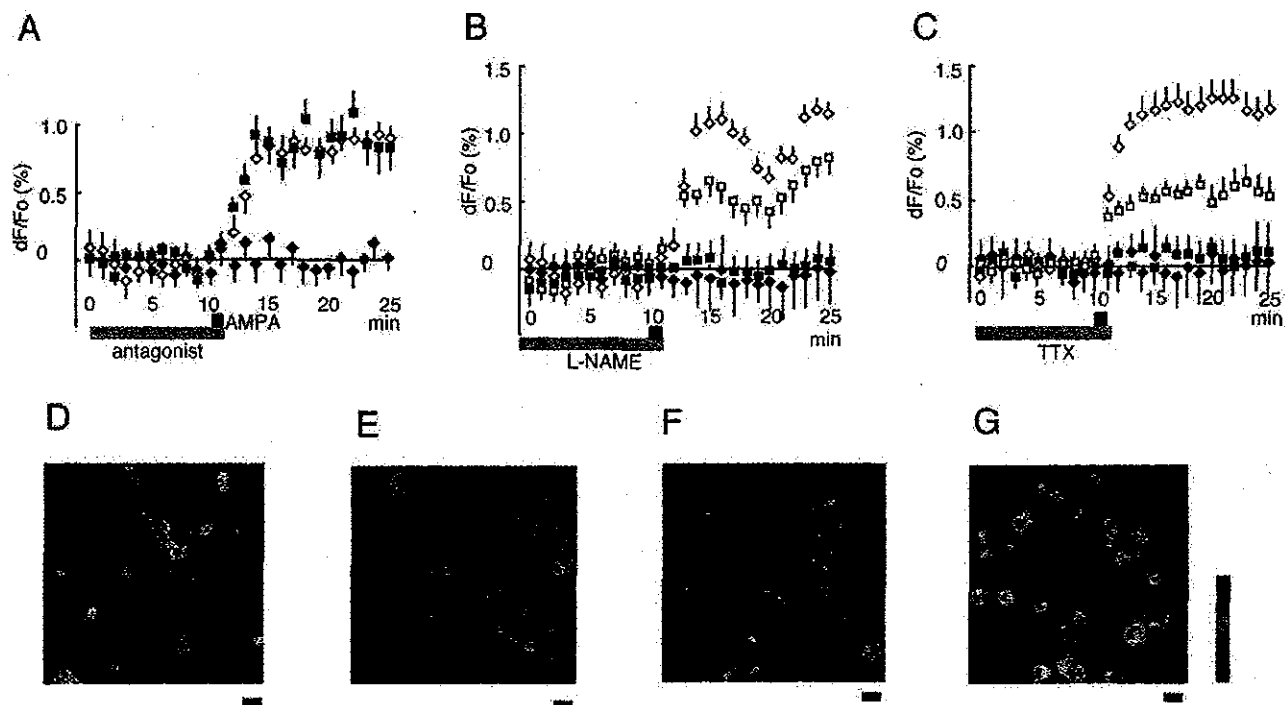
Fig. 5. AMPA receptor-dependent NO production. (A) Fluorescence increases evoked by AMPA (open diamonds, five ROIs from five slices) in ML of parasagittal slices were inhibited by CNQX (closed diamonds, five ROIs from four slices), but not by AP5 (closed squares, n=8 ROIs from two slices). Antagonists were applied during periods indicated by a blue bar, while a red bar indicates AMPA application. Averages and S.E.M. (vertical bars) of dF/Fo are shown. (B) Fluorescence increases evoked by AMPA in ML (open squares, four ROIs from four slices) and in GCL (open diamonds, two ROIs from two slices) of parasagittal slices were inhibited by L-NAME (ML, closed squares, four ROIs from four slices; GCL, closed diamonds, three ROIs from three slices). (C) Fluorescence increases evoked by 10 μM AMPA in ML (open squares, five ROIs from three slices) and GCL (open diamonds, two ROIs from two slices) of parasagittal slices were inhibited by 1 μM TTX (ML, closed squares, seven ROIs from six slices; GCL, closed diamonds, three ROIs from two slices). (D–G) Subtraction images (×40 objective, after−before 6 μM AMPA) of GCs in culture on DIV15. AMPA response in GC culture (D) was blocked by ω-conotoxin GVIA (1 μM, 10 min, E), or ω-agatoxin TK (0.1 μM, 10 min, F), but not by nifedipine (100 μM, 10 min, G). Scale bars=10 μm.

sis and NO production in cluster on fine fibers (n=4, Fig. 6E). Thus, Fig. 6C–E indicates that AMPA receptor activation produced NO in PF terminals.

Synergistic effect of NMDA and mGlu-1 receptors

NMDA at a higher concentration (100 μM) sometimes increased fluorescence in PC layer (PCL; n=3 of 9 slices). We therefore searched for the condition that could reproducibly evoke NO production in PCL, and found that electrical stimulation of WM at 50 Hz consistently increased fluorescence in PCL (n=6, Fig. 7Aa and Ac), while similar stimulation at 10 Hz did not (n=6, Fig. 7Ab and Ac). TTX (n=2, Fig. 7B) or L-NAME (n=4, not shown) blocked the fluorescence increase in PC. The frequency dependency suggested involvement of mGluR activation (Batchelor and Garthwaite, 1997). Actually, the 50 Hz-stimulation in the presence of 100 μM CPCCOEt, a selective blocker of mGlu-1 receptor (n=3, Fig. 7C), or D-AP5 (n=3, Fig. 7D) failed to increase fluorescence. As shown in Fig. 2B, (S)-DHPG alone increased fluorescence in GCL, but not in PCL. However, the 10 Hz-stimulation increased fluorescence in PCL in the presence of 100 μM (S)-DHPG (n=6, Fig. 7E). These results suggested that combined activation of NMDA and mGlu-1 receptors is necessary and sufficient for NO production in PCL. To show this critically, we ap-

plied 30 μM NMDA after a 10 min-application of 100 μM (S)-DHPG, and observed NO production in PCL (n=3, Fig. 7F).

PC soma does not express nNOS, but is surrounded by the axon terminal plexus of basket cell, the pinceau. Basket cells express NR-1 (ζ) and 2D (ϵ4) subunits of NMDA receptor (Watanabe et al., 1994; Petralia et al., 1994a,b), as well as mGlu-1 receptor (Baude et al., 1993), nNOS (Rodrigo et al., 1994) and PSD-95 (Hunt et al., 1996). Therefore, the fluorescence increase in PCL likely represents NO production in the pinceau triggered by synergistic activation of NMDA and mGlu-1 receptors. Co-application of (S)-DHPG and NMDA also synergistically increased cyclic GMP content in cerebellar slices. As shown in Fig. 7G, cyclic GMP level achieved by (S)-DHPG+NMDA was significantly higher than the simple summation of that achieved by each agonist alone (P<0.01, t-test, n=5). Either CPCCOEt (P<0.01) or D-AP5 (P<0.05) blocked the synergistic increase in cyclic GMP. These results showed that coactivation of NMDA and mGlu-1 receptors triggers synergistic NO production and increases cyclic GMP levels in cerebellar slices. Although the site of the synergistic cyclic GMP increase is not clear, this is likely to be triggered by synergistic activation of NOS in the pinceau.
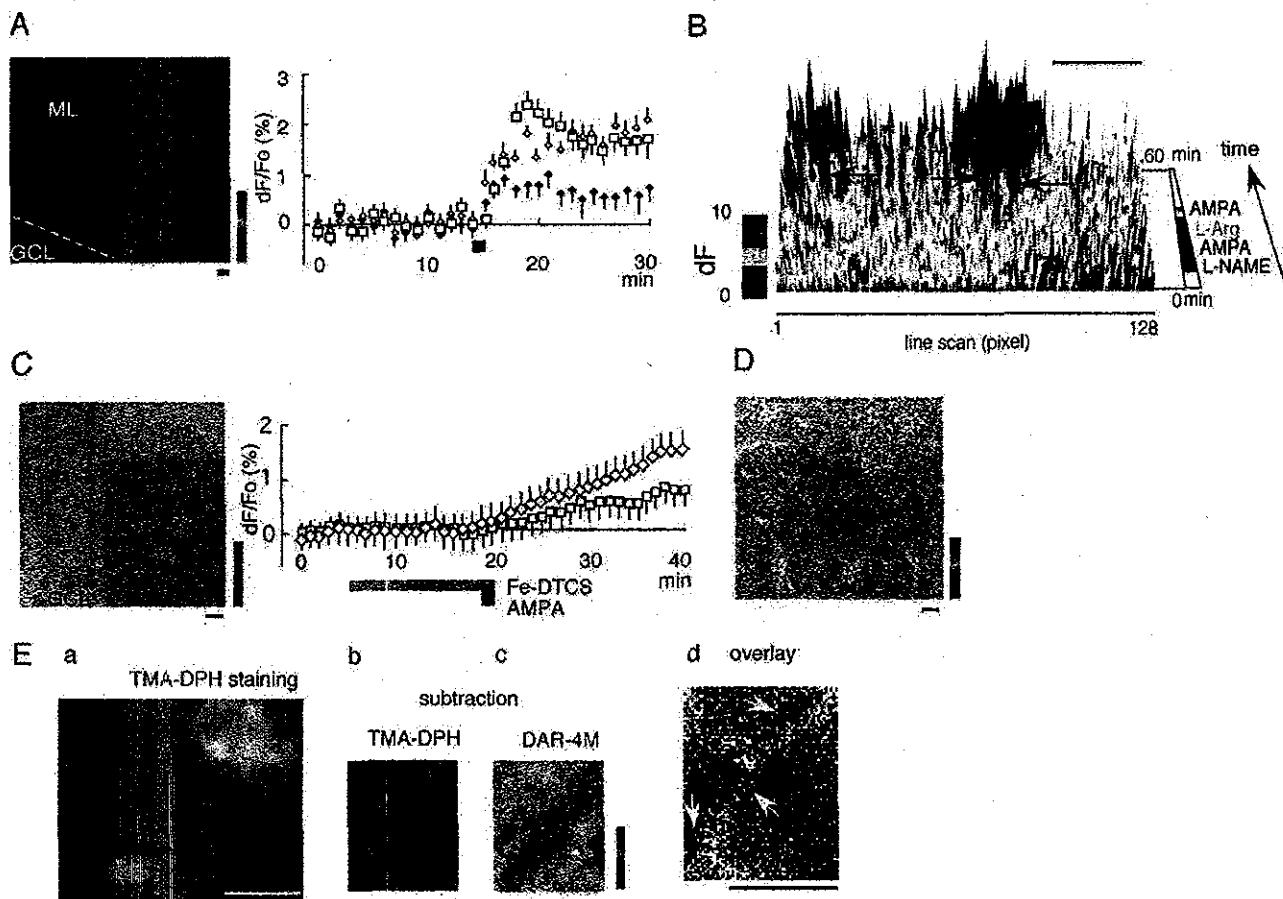
Fig. 6. AMPA receptor activation produces NO in PF terminals. (A, Left) A subtraction image (×40) showing response to AMPA of the parasagittal slice. Patches expressing larger fluorescent increase are seen in ML. Scale bar=10 μm. (Right) Averages and S.E.M. (vertical bars) of dF/Fo in several ROIs of three slices are shown. The red bar indicates AMPA application. Open diamonds: within patches in ML (five ROIs), closed diamonds: between patches in ML (eight ROIs), open squares: GCL (three ROIs). (B) Line-scan analysis of the intense fluorescent patch in ML. Images were taken every minute and a series of subtraction images from the initial picture were made. A linear ROI of 128-pixel long crossing a patch (horizontal axis) was selected and fluorescence change over time is indicated by pseudocolors. Scale bar=10 μm. Time course is expressed from the front to the back of the figure. Drugs were applied as indicated in the right. AMPA in the presence of L-NAME had no effect. L-Arginine (10 mM) was applied then the second challenge by AMPA increased fluorescence. The increase started from single pixels (arrows) and spread laterally. (C, Left) A subtraction image (×40 objective) showing that 100 μM Fe-DTCS (10 min) caused weak, uniform response to 10 μM AMPA in ML of a parasagittal slice (compare with Fig. 6A). The broken line indicates PCL. Scale bar=10 μm. (Right) Average and S.E.M. of dF/Fo in ML (open squares, n=6 ROI from three slices) and GCL (open diamonds, n=6 ROI from three slices) in the presence of Fe-DTCS. (D) A subtraction image (×10 objective) showing the response to 10 μM AMPA of GC culture in soma and fibers. Hot spots on fine fibers originated from the cell (below, left) are observed as red spots. Scale bar=10 μm. (E) Fluorescence increases in TMA-DPH (b) and DAR-4M (c) in a ROI (a) were binarized with a threshold at mean+2 S.D. TMA-DPH spots (green) and DAR-4M spots (red) were expressed as color dots and merged. This overlay figure (d) shows three clusters where both fluorescence dots are colocalized on a fiber (arrows), which are indicative of presynaptic production of NO. To emphasize changes on the fibers, only fluorescence on fibers were shown. Scale bars=10 μm.

DISCUSSION

The present study demonstrated that presynaptic NOS immuno-positive sites in the cerebellar cortex (Rodrigo et al., 1994), actually served as active NO sources. NO production in PF terminals depended exclusively on AMPA receptors. The AMPA receptor-dependent mechanism involves TTX-sensitive sodium channels and voltage-gated calcium channels, and produces low concentrations of NO presynaptically. This contrasts the NMDA receptor-dependent postsynaptic NO production, which releases NO via calcium entry through the receptor-coupled channel. In addition, we found that synergistic activation of NMDA and mGlu-1 receptors triggered NO

production in the pinceau. Together, these findings suggest that multiple gating receptor mechanisms govern NO production in specific neurons.

NO detection with DAF-2 fluorometry

DAF-2 diacetate is a membrane permeable, non-fluorescent compound. It is intracellularly converted to DAF-2, which in turn reacts with NO to produce a stable triazole compound, DAF-2T. This conversion is associated with a 250-fold increase in fluorescence, enabling sensitive (up to 5 nM *in vitro*) detection of NO (Kojima et al., 1998; Räthel et al., 2003). In tissues, however, the sensitivity may be reduced because light scattering and absorption interfere with fluorescence
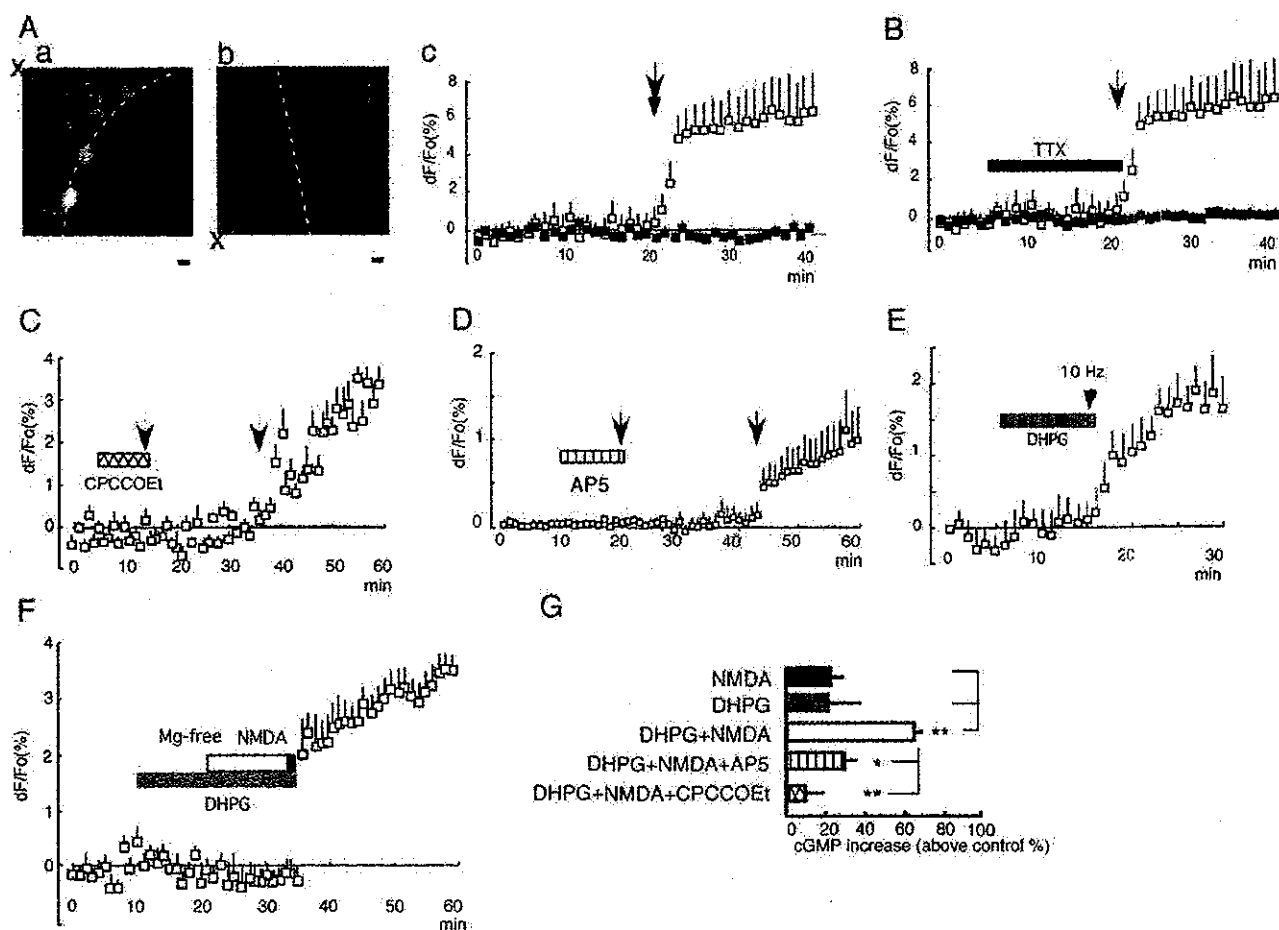
Fig. 7. Synergistic activation of NMDA and mGlu-1 receptors produces NO in PCL. (A) Subtraction images (×40 objective, after–before stimulation, parasagittal slices) showing that fluorescence spots appeared in PC soma after electric stimulation at 50 Hz (2 s, 30 V, Aa), but not at 10 Hz (Ab). The stimulation electrode was placed in WM (marked by X). (Ac) Average and S.E.M. of dF/Fo in a PC soma. The arrow (50 Hz) or arrowhead (10 Hz) indicates stimulation. Open squares: 50 Hz (six ROIs from six slices), closed squares: 10 Hz (six ROIs from six slices). (B) Fluorescence was not increased by 50 Hz stimulation (arrow) in the presence of 1 μM TTX (closed bar). Averages and S.E.M. of dF/Fo in four ROIs from three slices are shown. Open squares: without TTX, the same data as in Ac. Closed squares: with TTX. (C) Stimulation at 50 Hz (arrows) did not increase fluorescence in PC soma in the presence of 30 μM CPCCOEt (hatched bar). Averages and S.E.M. of dF/Fo in five ROIs from three slices are shown. (D) Stimulation at 50 Hz (arrows) did not increase fluorescence in PC soma in the presence of 50 μM D-AP5 (hatched bar). Averages and S.E.M. of dF/Fo in five ROIs from three slices are shown. (E) Stimulation at 10 Hz (arrowheads) increased fluorescence in PC soma in the presence of 100 μM (S)-DHPG (shaded bar). Averages and S.E.M. of dF/Fo in 15 ROIs from six slices are shown. (F) Soma response was evoked by 30 μM NMDA (closed bar, open bar indicates Mg-free ACSF) primed by 100 μM (S)-DHPG (shaded bar). Averages and S.E.M. of dF/Fo in nine ROIs from three slices are shown. (G) Accumulation of cyclic GMP measured by enzyme-linked immunoassay of slice extract. Slices were incubated with 0.1 mM 3-isobutyl-1-methylxanthine from 5 min prior to addition of agonists. ** $P < 0.01$, * $P < 0.05$. Averages and S.E.M. of five slices are shown.

detection. Nitrite, nitrate, superoxide, hydrogen peroxide and divalent cations such as calcium and magnesium do not affect DAF-2 fluorescence (Kojima et al., 1998; Suzuki et al., 2002). Although dehydroascorbic acid and ascorbic acid increased DAF-2 fluorescence, the reaction requires these compounds at concentrations >mM (Zhang et al., 2002). Thus, NO specifically converts DAF-2 into DAF-2T in living tissues.

It was reported that oxidation of DAF-2 by peroxynitrite (Jourd'heuil, 2002) or intense light (Broillet et al., 2001) also increased its fluorescence. However, peroxynitrite generation in cells requires NO production, and intense light increases DAF-2 fluorescence only in the presence of NO. Therefore, although these reactions might enhance fluorescence when NO is produced, they do not disguise

the fact of NO production. We constantly confirmed NOS-dependent NO production using a NOS inhibitor.

It is, however, noteworthy that quantitative measurements of NO concentrations within tissues, such as direct comparison of NO concentrations between areas, are beyond the ability of DAF-2 fluorometry, because conversion of DAF-2 into DAF-2T is not accompanied with spectral shift, preventing calibration by 2-wavelengths measurement. We concluded that the unit NO release was much less in ML, based on the observation that a detectable fluorescence increase in ML required more numbers of stimuli than other areas (Fig. 1).

DAF-2T fluorescence depicts diffusion-based spread of NO around active NO sources (Fig. 6B). Distributions of DAF-2 and DAF-2T were uniform within a cell (Fig. 1). NO

spreading area would merge together where weak NO sources are present at high density (Lancaster, 1994). This diffusibility of NO, together with light scattering by slice thickness, lowers contrast of our fluorescence images, preventing precise identification of individual active NO sources. However, the use of dispersed cells or an extracellular NO scavenger reduced this ambiguity. Furthermore, differential fluorescence intensity due to membrane density difference among layers enabled discrimination of each layers.

Reaction of DAF-2 with NO occurs within several seconds (Kojima et al., 1998). Since DAF-2T is stable in cells (Kojima et al., 1998), growth of DAF-2T fluorescence over time provides a cumulative map of NO generation in the tissue. Agonist permeation across slice thickness may cause continuous growth of fluorescence after cessation of agonist application observed in some figures such as Fig. 6C.

NMDA-dependent NO production

The NMDA receptor-coupled mechanism activates nNOS close to the receptor. Although it was reported that NO production evoked by 300 μM NMDA in the presence of Mg^{2+} ions was TTX-sensitive (Southam et al., 1991), it was TTX-insensitive in the absence of Mg^{2+} ions in our hands. Since we used lower concentrations of NMDA (30 μM), it is suggested that the effects of NMDA are dose-dependent; both TTX-sensitive and -insensitive components would be activated at higher concentration, while lower concentrations of NMDA activate only postsynaptic NO production.

The discontinuous patterning of NO production was also found by histochemical experiments of nNOS, NADPH-diaphorase (Hawkes and Turner, 1994; Yan et al., 1993) and cGMP (DeVente et al., 1990). This sagittal band is developed in a manner dependent on the pattern of the mossy fiber inputs (Oberdick et al., 1998). Since NMDA activates nNOS in the postsynaptic density complex, it is likely that the banding pattern represents a partial fraction of nNOS linked to NMDA receptors in postsynaptic sites. In contrast, observation of uniform NO production throughout GCL suggests a possibility that a population of nNOS localized extrasynaptically is linked to AMPA and mGlu-1 receptors.

NO production in ML

NO production in ML increases cyclic GMP levels in PCs (Hartell et al., 2001), which is critical for long-term depression of PF synapses (Shibuki and Okada, 1991; Lev-Ram et al., 1995). It has been reported that PF activities produced NO in ML (Shibuki and Kimura, 1997; Casado et al., 2000; Hartell et al., 2001), although responsible receptors were controversial. The present study demonstrated that AMPA receptor is the major trigger of NO production in ML, which causes depolarization of GC and calcium influx in PF terminals through opening voltage-gated calcium channels. These results are consistent with our previous observation (Hartell et al., 2001).

In contrast to NMDA-dependent mechanism, AMPA receptor-dependent NO production was entirely sensitive to TTX and dependent on high-threshold calcium channels, implying the indirect coupling of AMPA receptor with remote nNOS through conduction of depolarization. Molecular organization of such an indirect coupling (for example, relative distance between the receptor and nNOS, or how calcium channels and nNOS are coupled) remains to be investigated; however, our observations indicate that such a "remote" mechanism is important in axonal production of NO, which works as a neuronal output. This contrasts the postsynaptic NO production that functions as one of the elements of dendritic computation. Thus, AMPA- and NMDA-dependent mechanisms generate NO carrying distinct computational information (Garthwaite, 1991).

The present study indicated that the gate-receptors regulate initial NO concentrations. Close linkage between NMDA receptor and nNOS allows NO production at a near-maximal rate, while the indirect activation gated by AMPA receptor does not. Theoretical works (Wood and Garthwaite, 1994; Lancaster, 1994) estimated that NO generated by NMDA receptor-dependent full activation of nNOS spreads over 100 μm, which contains about 5×10^4 synapses in ML, judged from the reported density of spines (Ito, 1984). In contrast, brighter patches representing intercellular diffusion of NO originated from PF terminals (Fig. 6) had a radius of 5 μm and may contain 420 PC spines. Since the number of the NO-generating PFs present in a patch is not necessarily 1, NO diffusion distance from a single source may be less than 5 μm, which is much less than expected from NMDA receptor-dependent mechanism. Since above estimation depends on the detection limit of DAF-2T fluorescence, precise estimation of NO diffusion in tissue requires further efforts. Nevertheless, we suggest that recruitment of the AMPA receptor-dependent mechanism limits the number of the affected synapses. Low initial concentrations of NO may delimit regions that undergo plastic changes in synaptic transmission. Modulation of input specificity of synaptic function by a diffusible messenger sounds paradoxical; however, it might be important for error-tolerant processing by neuronal circuit.

Synergistic production of NO in the pinceau

NO production in the pinceau was observed only after specific pharmacological or electrical stimuli: coactivation of mGlu-1 receptor with NMDA receptor, but not AMPA receptor (Okada, 1992), or electrical stimulation at 50 Hz, but not at 10 Hz. It is thus suggested that specific neuronal inputs activate nNOS in the pinceau through a TTX-sensitive "remote" mechanism. Since mGlu-1 receptor is always found in postsynaptic sites (Baude et al., 1993), nNOS activation in the pinceau may involve modification of NMDA receptor current or intracellular calcium dynamics by mGlu-1 receptor (Skeberdis et al., 2001). Basket cells regulate excitability of PCs through strong inhibitory transmission, and our observation of NO production in the pinceau indicates that NO is released together with GABA.

Therefore, it is possible that NO from the pinceau modulates GABA function through GABA-A receptor phosphorylation or GABA transporter inhibition (Robello et al., 1996; Shen et al., 1997). As another possibility, NO from this site may affect gene expression in PC (Peunova and Enikolopov, 1993; Gudi et al., 2000).

REFERENCES

Batchelor AM, Garthwaite J (1997) Frequency detection and temporally dispersed synaptic signal association through a metabotropic glutamate receptor pathway. Nature 385:74–77.

Baude A, Nusser Z, Roberts JDB, Mulvihill E, McIlhinney RAJ, Somogyi P (1993) The metabotropic glutamate receptor (mGluR1) is concentrated at perisynaptic membrane of neuronal subpopulations as detected by immunogold reaction. Neuron 11:771–787.

Boehme GA, Bon C, Stutzman J-M, Doble A, Blanchard J-C (1991) Possible involvement of nitric oxide in long-term potentiation. Eur J Pharmacol 199:379–381.

Bredt DS, Snyder SH (1989) Nitric oxide mediates glutamate-linked enhancement of cGMP levels in the cerebellum. Proc Natl Acad Sci USA 86:9030–9033.

Bredt DS, Snyder SH (1990) Isolation of nitric oxide synthase, a calmodulin-requiring enzyme. Proc Natl Acad Sci USA 87:682–685.

Brenman JE, Chao DS, Gee SH, McGee AW, Craven SE, Santillano DR, Wu A, Huang F, Xia H, Peters MF, Froehner SC, Bredt DS (1996) Interaction of nitric oxide synthase with the postsynaptic density protein PSD-95 and α1-syntrophin mediated by PDZ domains. Cell 84:757–767.

Broillet M-C, Randin O, Chatton J-Y (2001) Photoactivation and calcium sensitivity of the fluorescent NO indicator 4,5-diaminofluorescein (DAF-2): implications for cellular NO imaging. FEBS Lett 491:227–232.

Bronner C, Landry Y, Fonteneau PA, Kuhry JG (1986) Fluorescent hydrophobic probe used for monitoring the kinetics of exocytosis phenomena. Biochemistry 25:2149–2154.

Calabresi P, Gubellini P, Centonze D, Sancesario G, Morello M, Giorgi M, Pisani A, Bernardi G (1999) A critical role of the nitric oxide/cGMP pathway in corticostriatal long-term depression. J Neurosci 19:2489–2499.

Casado M, Dieudonne S, Ascher P (2000) Presynaptic N-methyl-D-aspartate receptors at the parallel fiber-Purkinje cell synapse. Proc Natl Acad Sci USA 97:11593–11597.

Christopherson KS, Hillier BJ, Lim WA, Bredt DS (1999) PSD-95 assembles a ternary complex with the N-methyl-D-aspartic acid receptor and a bivalent neuronal NO synthase PSD domain. J Biol Chem 274:27467–27473.

Crepel F, Audinat E, Daniel H, Hemart N, Jaillard D, Rossier J, Lambolez B (1994) Cellular locus of the nitric oxide-synthase involved in cerebellar long-term depression induced by high external potassium concentration. Neuropharmacology 33:1399–1405.

DeVente J, Bol JGJM, Berkelmans HS, Schipper J, Steinbusch HMW (1990) Immunocytochemistry of cGMP in the cerebellum of the immature, adult, and aged rat: the involvement of nitric oxide: a micropharmacological study. Eur J Neurosci 2:845–862.

Förstermann U, Gath I (1996) Purification of isoforms of nitric oxide synthase. Methods Enzymol 268:334–349.

Fujii S, Suzuki Y, Yoshimura T, Kamada H (1998) In vivo three-dimensional EPR imaging of nitric oxide production from isosorbide dinitrate in mice. Am J Physiol 274:G857–862.

Furuya S, Makino A, Hirabayashi Y (1998) An improved method for

culturing cerebellar Purkinje cells with differentiated dendrites under a mixed monolayer setting. Brain Res Protocols 3:192–198.

Gally JA, Montague PR, Reeke GN, Edelman GM (1990) The NO hypothesis: possible effects of a short-lived, rapidly diffusible signal in the development and function of the nervous system. Proc Natl Acad Sci USA 87:3547–3551.

Garthwaite J, Charles SL, Chess-Williams C (1988) Endothelium-derived relaxing factor release on activation of NMDA receptors suggests role as intercellular messenger in the brain. Nature 336:385–388.

Garthwaite J (1991) Glutamate, nitric oxide and cell-cell signalling in the nervous system. Trends Neurosci 14:60–67.

Gudi T, Casteel DE, Vinson C, Ross GR, Pilz RB (2000) NO activation of fos promoter elements requires nuclear translocation of G-kinase and CREB phosphorylation but is independent of MAP kinase activation. Oncogene 19:6324–6333.

Hartell NA (1996) Strong activation of parallel fibers produces localized calcium transients and a form of LTD that spreads to distant synapses. Neuron 16:801–810.

Hartell NA, Furuya S, Jacoby S, Okada D (2001) Intercellular action of nitric oxide increases cGMP in cerebellar Purkinje cells. Neuroreport 12:25–28.

Hawkes H, Turner RW (1994) Compartmentation of NADPH-diaphorase activity in the mouse cerebellar cortex. J Comp Neurol 346:499–516.

Hunt CA, Schenker LJ, Kennedy MB (1996) PSD-95 is associated with the postsynaptic density and not with the presynaptic membrane at forebrain synapses. J Neurosci 16:1380–1388.

Ito M (1984) The cerebellum and neural control. New York: Raven Press.

Jourd'heuil D (2002) Increased nitric oxide-dependent nitrosylation of 4,5-diaminofluorescein by oxidants: implications for the measurement of intracellular nitric oxide. Free Radic Biol Med 33:676–684.

Kimura S, Uchiyama S, Takahashi HE, Shibuki K (1998) cAMP-dependent long-term potentiation of nitric oxide release from cerebellar parallel fibers in rats. J Neurosci 18:8551–8558.

Kojima H, Nakatsubo N, Kikuchi K, Kawahara S, Kirino Y, Nagoshi H, Hirata Y, Nagano T (1998) Detection and imaging of nitric oxide with novel fluorescent indicators: diaminofluoresceins. Anal Chem 70:2446–2453.

Kojima H, Hirotani M, Nakatsubo N, Kikuchi K, Urano Y, Higuchi T, Hirata Y, Nagano T (2001) Bioimaging of nitric oxide with fluorescent indicators based on rhodamine chromophore. Anal Chem 73:1967–1973.

Krekelberg B, Taylor JG (1996) Nitric oxide in cortical map formation. J Chem Neuroanat 10:191–196.

Lancaster JR (1994) Simulation of the diffusion and reaction of endogenously produced nitric oxide. Proc Natl Acad Sci USA 91:8137–8141.

Lev-Ram V, Makings LR, Keitz PF, Kao JP, Tsien RY (1995) Long-term depression in cerebellar Purkinje neurons results from coincidence of nitric oxide and depolarization-induced Ca^{2+} transients. Neuron 15:407–415.

Malinski T, Taha Z (1992) Nitric oxide release from a single cell measured in situ by a porphyrinic-based microsensor. Nature 358:676–678.

Miyata M, Okada D, Hashiimoto K, Kano M, Ito M (1999) Corticotropin-releasing factor plays a permissive role in cerebellar long-term depression. Neuron 22:763–775.

Oberdick J, Baader SL, Schilling K (1998) From zebra stripes to postal zones: deciphering patterns of gene expression in the cerebellum. Trends Neurosci 21:383–390.

Okada D (1992) Two pathways of cyclic GMP production through glutamate receptor mediated nitric oxide synthesis. J Neurochem 59:1203–1210.

Okada D (2000) Neutral red as a hydrophobic probe for neuronal activity monitoring. J Neurosci Methods 101:85–92.

Petralia RS, Yokotani N, Wenthold RJ (1994a) The NMDA receptor subunits NR2A and NR2B show histological and ultrastructural

localization patterns similar to those of NR1. J Neurosci 14:6102–6120.

Petralia RS, Yokotani N, Wenthold RJ (1994b) Light and electron microscope distribution of the NMDA receptor subunit NMDAR1 in rat nervous system using a selective anti-peptide antibody. J Neurosci 14:667–696.

Peunova N, Enikolopov G (1993) Amplification of calcium-induced gene transcription by nitric oxide in neuronal cells. Nature 364:450–453.

Räthel TR, Leikert JF, Vollmar AM, Dirsch VM (2003) Application of 4,5-diaminofluorescein to reliably measure nitric oxide released from endothelial cells in vitro. Biol Proc Online 5:136–142.

Robello M, Amico C, Bucossi G, Cupello A, Rapalino MV, Thellung S (1996) Nitric oxide and GABAA receptor function in the rat cerebral cortex and cerebellar granule cells. Neuroscience 74:99–105.

Rodrigo J, Springall DR, Uttenthal O, Bentura ML, Abadia-Molina F, Riveros-Moreno V, Martinez-Murillo R, Polak JM, Moncada S (1994) Localization of nitric oxide synthase in the adult rat brain. Phil Trans R Soc Lond B 345:175–221.

Sattler R, Xiong Z, Lu W-Y, Hafner M, MacDonald JF, Tymianski M (1999) Specific coupling of NMDA receptor activation to nitric oxide neurotoxicity by PSD-95 protein. Science 284:1845–1848.

Schuman EM, Madison DV (1994) Nitric oxide and synaptic function. Annu Rev Neurosci 17:153–183.

Shen KZ, Cox BA, Johnson SW (1997) L-Arginine potentiates GABA-mediated synaptic transmission by a nitric oxide-dependent mechanism in rat dopamine neurons. Neuroscience 79:649–658.

Shibuki K, Kimura S (1997) Dynamic properties of nitric oxide release from parallel fibres in rat cerebellar slices. J Physiol (Lond) 498:443–452.

Shibuki K, Okada D (1991) Endogenous nitric oxide release required

for long-term synaptic depression in the cerebellum. Nature 349:326–328.

Skeberdis VA, Lan J, Opitz T, Zheng X, Bennett MV, Zukin RS (2001) mGluR1-mediated potentiation of NMDA receptors involves a rise in intracellular calcium and activation of protein kinase C. Neuropharmacology 40:856–865.

Southam E, East SJ, Garthwaite J (1991) Excitatory amino acid receptors coupled to the nitric oxide/cyclic GMP pathway in rat cerebellum during development. J Neurochem 56:2072–2081.

Suzuki N, Kojima H, Urano Y, Kikuchi K, Hirata Y, Nagano T (2002) Orthogonality of calcium concentration and ability of 4,5-diaminofluorescein to detect NO. J Biol Chem 277:47–49.

Tanaka M, Yoshida S, Yano M, Hanaoka F (1994) Roles of endogenous nitric oxide in cerebellar cortical development in slice cultures. Neuroreport 5:2049–2052.

Watanabe M, Mishina M, Inoue Y (1994) Distinct spatiotemporal expressions of five NMDA receptor channel subunit mRNAs in the cerebellum. J Comp Neurol 343:513–519.

Wood J, Garthwaite J (1994) Models of the diffusional spread of nitric oxide: implications for neural nitric oxide signalling and its pharmacological properties. Neuropharmacology 33:1235–1244.

Wu HH, Williams CV, McLoon SC (1994) Involvement of nitric oxide in the elimination of a transient retinotectal projection in development. Science 265:1593–1596.

Yan XX, Jen LS, Garey LJ (1993) Parasagittal patches in the granular layer of the developing and adult rat cerebellum as demonstrated by NADPH-diaphorase histochemistry. Neuroreport 4:1227–1230.

Zhang X, Kim WS, Hatcher N, Potgieter K, Moroz LL, Gillette R, Sweedler JV (2002) Interfering with nitric oxide measurements: 4,5-diaminofulorescein reacts with dehydroascorbic acid and ascorbic acid. J Biol Chem 277:48472–48478.

J|A|C|S

A R T I C L E S

Development of a Zinc Ion-Selective Luminescent Lanthanide Chemosensor for Biological Applications

Kenjiro Hanaoka,[†] Kazuya Kikuchi,*,[†,‡] Hirotatsu Kojima,[†] Yasuteru Urano,[†] and Tetsuo Nagano*,[†]

*Contribution from the Graduate School of Pharmaceutical Sciences,
The University of Tokyo, 7-3-1 Hongo, Bunkyo-ku, Tokyo 113-0033, Japan,
and Presto, JST Corporation, Kawaguchi, Saitama 332-0012, Japan*

Received May 25, 2004; E-mail: tlong@mol.f.u-tokyo.ac.jp (T.N.); kkikuchi@mol.f.u-tokyo.ac.jp (K.K.)

Abstract: Detection of chelatable zinc (Zn^{2+}) in biological studies has attracted much attention recently, because chelatable Zn^{2+} plays important roles in many biological systems. Lanthanide complexes (Eu^{3+}, Tb^{3+}, etc.) have excellent spectroscopic properties for biological applications, such as long luminescence lifetimes of the order of milliseconds, a large Stoke's shift of >200 nm, and high water solubility. Herein, we present the design and synthesis of a novel lanthanide sensor molecule, **[Eu-7]**, for detecting Zn^{2+}. This europium (Eu^{3+}) complex employs a quinolyl ligand as both a chromophore and an acceptor for Zn^{2+}. Upon addition of Zn^{2+} to a solution of **[Eu-7]**, the luminescence of Eu^{3+} is strongly enhanced, with high selectivity for Zn^{2+} over other biologically relevant metal cations. One of the important advantages of **[Eu-7]** is that this complex can be excited with longer excitation wavelengths (around 340 nm) as compared with previously reported Zn^{2+}-sensitive luminescent lamthanide sensors, whose excitation wavelength is at too high an energy level for biological applications. The usefulness of **[Eu-7]** for monitoring Zn^{2+} changes in living HeLa cells was confirmed. This novel Zn^{2+}-selective luminescent lanthanide chemosensor **[Eu-7]** should be an excellent lead compound for the development of a range of novel luminescent lanthanide chemosensors for biological applications.

Introduction

Zinc (Zn^{2+}) is the second most abundant heavy metal ion after iron in the human body, and the total zinc ion concentration in serum is of the order of 10 μM.[1] Zn^{2+} is an essential component of many enzymes (e.g., carbonic anhydrase), and also plays critical roles in maintaining key structural features of gene transcription proteins (e.g., zinc finger proteins).[2] Moreover, chelatable Zn^{2+} is present at especially high concentrations in brain,[3] pancreas,[4] and spermatozoa.[5] Chelatable Zn^{2+} regulates neuronal transmission in excitatory nerve terminals,[3] suppresses apoptosis,[6] contributes to neuronal injury in certain acute conditions,[7] epilepsy,[8] and transient global ischemia,[9] and induces the formation of β-amyloid,[10] which is reported to be related to

the etiology of Alzheimer's disease. Although many reports describe the significance of chelatable Zn^{2+} in biological systems, its mechanisms of action are less well understood than those of other cations, such as Ca^{2+}, Na^+, and K^+. Therefore, there is considerable interest in detecting chelatable Zn^{2+} in biological systems.[11]

So far, several Zn^{2+}-selective fluorescent sensor molecules have been reported.[12] However, novel types of Zn^{2+}-sensitive fluorescent sensor molecules are needed for studies on biological phenomena, and several new types of sensors that are designed for ratiometric measurement,[13] or that are peptide- or protein-based,[14] have recently been introduced. Ratiometric measure-
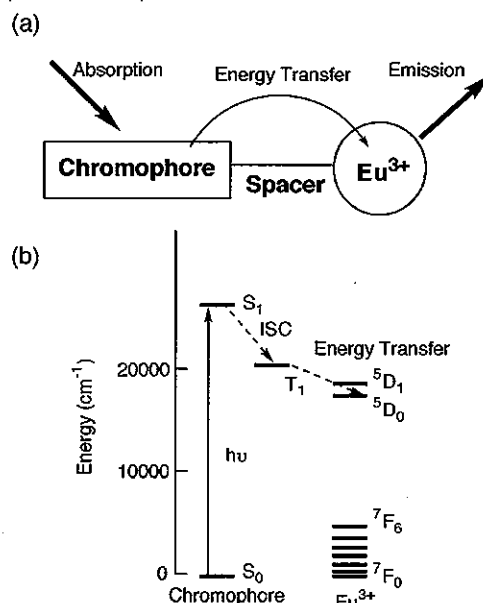
[†] The University of Tokyo.

[‡] Presto, JST Corporation.

(1) Paker, M. M.; Humaller, F. L.; Mahler, D. J. *Clin. Chem.* **1967**, *13*, 40–48.

(2) (a) Vallee, B. L.; Falchuk, K. H. *Physiol. Rev.* **1993**, *73*, 79–118. (b) Berg, J. M.; Shi, Y. *Science* **1996**, *271*, 1081–1085.

(3) Frederickson, C. J. *Int. Rev. Neurobiol.* **1989**, *31*, 145–238.

(4) Zalewski, P. D.; Millard, S. H.; Forbes, I. J.; Kapaniris, O.; Slavotinek, A.; Betts, W. H.; Ward, A. D.; Lincoln, S. F.; Mahadevan, I. *J. Histochem. Cytochem.* **1994**, *42*, 877–884.

(5) Zalewski, P. D.; Jian, X.; Soon, L. L. L.; Breed, W. G.; Seamark, R. F.; Lincoln, S. F.; Ward, A. D.; Sun, F. Z. *Reprod. Fertil. Dev.* **1996**, *8*, 1097–1105.

(6) Truong-Tran, A. Q.; Ho, L. H.; Chai, F.; Zalewski, P. D. *J. Nutr.* **2000**, *130*, 1459S-1466S.

(7) Choi, D. W.; Koh, J. Y. *Annu. Rev. Neurosci.* **1998**, *21*, 347–375.

(8) Frederickson, C. J.; Hernandez, M. D.; McGinty, J. F. *Brain Res.* **1989**, *480*, 317–321.

(9) Koh, J. Y.; Suh, S. W.; Gwag, B. J.; He, Y. Y.; Hsu, C. Y.; Choi, D. W. *Science* **1996**, *272*, 1013–1016.

(10) Bush, A. I.; Pettingell, W. H.; Multhaup, G.; Paradis, M. D.; Vonsattel, J. P.; Gusella, J. F.; Beyreuther, K.; Masters, C. L.; Tanzi, R. E. *Science* **1994**, *265*, 1464–1467.

(11) (a) Kikuchi, K.; Komatsu K.; Nagano T. *Curr. Opin. Chem. Biol.* **2004**, *8*, 182–191. (b) Jiang, P.; Guo, Z. *Coord. Chem. Rev.* **2004**, *248*, 205–229.

(12) (a) Frederickson, C. J.; Kasarskis, E. J.; Ringo, D.; Frederickson, R. E. *J. Neurosci. Methods* **1987**, *20*, 91–103. (b) Zalewski, P. D.; Forbes, I. J.; Betts, W. H. *Biochem. J.* **1993**, *296*, 403–408. (c) Hirano, T.; Kikuchi, K.; Urano, Y.; Nagano, T. *J. Am. Chem. Soc.* **2002**, *124*, 6555–6562. (d) Walkup, G. K.; Burdette, S. C.; Lippard, S. J.; Tsien, R. Y. *J. Am. Chem. Soc.* **2000**, *122*, 5644–5645. (e) Haugland, R. P. *Handbook of Fluorescent Probes and Research Chemicals*, 6th ed.; Molecular Probes, Inc.; Eugene, OR, 1996; (f) Hendrickson K. M.; Geue, J. P.; Wyness, O.; Lincoln, S. F.; Ward, A. D. *J. Am. Chem. Soc.* **2003**, *125*, 3889–3895. (g) Gee, K. R.; Zhou, Z. L.; Qian, W. J.; Kennedy, R. *J. Am. Chem. Soc.* **2002**, *124*, 776–778. (h) Burdette, S. C.; Frederickson, C. J.; Bu, W.; Lippard, S. J. *J. Am. Chem. Soc.* **2003**, *125*, 1778–1787.

(13) (a) Henary, M. M.; Wu, Y.; Fahrni, C. J. *Chem. Eur. J.* **2004**, *10*, 3015–3025. (b) Taki, M.; Wolford, J. L.; O'Halloran, T. V. *J. Am. Chem. Soc.* **2004**, *126*, 712–713. (c) Woodroofe, C. C.; Lippard, S. J. *J. Am. Chem. Soc.* **2003**, *125*, 11458–11459. (d) Maruyama, S.; Kikuchi, K.; Hirano, T.; Urano, Y.; Nagano, T. *J. Am. Chem. Soc.* **2002**, *124*, 10650–10651.

ment in particular enables more precise analysis of Zn^{2+} concentrations. The other approach for precise analyses is time-resolved fluorescence (TRF) measurement, which offers a better signal-to-noise ratio. Luminescent lanthanide complexes are suitable for TRF measurement. So, our interest in Zn^{2+}-selective fluorescent sensor molecules was directed toward luminescent lanthanide complexes, in particular complexes of the europium and terbium trivalent ions (Eu^{3+} and Tb^{3+}). These complexes have large Stoke's shifts (>200 nm), long luminescence lifetimes of the order of milliseconds, and high water solubility,[15] whereas the typical organic fluorescent compounds possess small Stoke's shifts (Stoke's shifts of fluorescein and rhodamine are ~25 and ~20 nm, respectively)[12c-e,16] and short fluorescence lifetimes in the nanosecond region. The long-lived luminescence of the lanthanides has the advantage that short-lived background fluorescence and scattered light decay to negligible levels when a pulse of excitation light is applied and the emitted light is collected after an appropriate delay time. For these reasons, sensitization of lanthanide luminescence has been exploited for a number of useful signaling systems for time-resolved assays in the fields of medicine, biotechnology, and biological science.[17] The lanthanide f–f transitions have low absorbance, so the ligand structure requires a sensitizing chromophore for high luminescence.[18] Absorption by the chromophore results in effective population of its triplet level, and efficient intramolecular energy transfer occurs from the excited chromophore to the lanthanide metal, whereby the metal becomes excited to the emission state (Scheme 1).[15a,17g,18b] By means of appropriate chromophore design, it is possible to develop luminescent lanthanide complexes which can be used to sense various biological molecules.

There are only a few reports about lanthanide-based luminescent chemosensors for the detection of Zn^{2+}.[19] Parker and co-workers have developed a luminescent lanthanide agent which binds Zn^{2+} with an apparent dissociation constant K_d of 0.6 μM (295 K, pH 7.3).[19a,c] We employed a different design approach for a ligand and an antenna in a previous report, and

(14) (a) Thompson, R. B.; Cramer, M. L.; Bozym, R.; Fierke, C. A. *J. Biomed. Opt.* **2002**, *7*, 555−560. (b) Shults, M. D.; Pearce, D. A.; Imperiali, B. *J. Am. Chem. Soc.* **2003**, *125*, 10591−10597. (c) Barondeau, D. P.; Kassmann, C. J.; Tainer, J. A.; Getzoff, E. D. *J. Am. Chem. Soc.* **2002**, *124*, 3522−3524.

(15) (a) Parker, D.; Williams, J. A. G. *J. Chem. Soc., Dalton Trans.* **1996**, 3613−3628. (b) Li, M.; Selvin, P. R. *J. Am. Chem. Soc.* **1995**, *117*, 8132−8138. (c) Beck, J. B.; Rowan, S. J. *J. Am. Chem. Soc.* **2003**, *125*, 13922−13923. (d) Franz, K. J.; Nitz, M.; Imperiali, B. *ChemBioChem* **2003**, *4*, 265−271. (e) Liu, W.; Jiao, T.; Li, Y.; Liu, Q.; Tan, M.; Wang, H.; Wang, L. *J. Am. Chem. Soc.* **2004**, *126*, 2280−2281. (f) Weibel, N.; Charbonnière, L. J.; Guardigli, M.; Roda, A.; Ziessel, R. *J. Am. Chem. Soc.* **2004**, *126*, 4888−4896. (g) Alpha, B.; Lehn, J. M.; Mathis, G. *Angew. Chem., Int. Ed. Engl.* **1987**, *26*, 266−267. (h) Petoud, S.; Cohen, S. M.; Bünzli, J. C. G.; Raymond, K. N. *J. Am. Chem. Soc.* **2003**, *125*, 13324−13325. (i) Maffeo, D.; Williams, J. A. G. *Inorg. Chim. Acta* **2003**, *355*, 127−136.

(16) Mizukami, S.; Kikuchi, K.; Higuchi, T.; Urano, Y.; Mashima, T.; Tsuruo, T.; Nagano, T. *FEBS Lett.* **1999**, *453*, 356−360.

(17) (a) Kolb, A. J.; Kaplita, P. V.; Hayes, D. J.; Park, Y. W.; Pernell, C.; Major, J. S.; Mathis, G *Drug Discovery Today* **1998**, *3*, 333−342. (b) Enomoto, K.; Araki, A.; Nakajima, T.; Ohta, H.; Dohi, K.; Préaudat, M.; Seguin, P.; Mathis, G.; Suzuki, R.; Kominami, G.; Takemoto, H. *J. Pharm. Biomed. Anal.* **2002**, *28*, 73−79. (c) Beeby, A.; Botchway, S. W.; Clarkson, I. M.; Faulkner, S.; Parker, A. W.; Parker, D.; Williams, J. A. G. *J. Photochem. Photobiol. B: Biology* **2000**, *57*, 83−89. (d) Frias, J. C.; Bobba, G.; Cann, M. J.; Hutchison, C. J.; Parker, D. *Org. Biomol. Chem.* **2003**, *1*, 905−907. (e) Barrios, A. M.; Craik, C. S. *Bioorg. Med. Chem. Lett.* **2002**, *12*, 3619−3623. (f) Vereb, G.; Jares-Erijman, E.; Selvin, P. R.; Jovin, T. M. *Biophys. J.* **1998**, *74*, 2210−2222. (g) Matsumoto, K.; Nojima, T.; Sano, H.; Majima, K. *Macromol. Symp.* **2002**, *186*, 117−121. (h) Karvinen, J.; Hurskainen, P.; Gopalakrishnan, S.; Burns, D.; Warrior, U.; Hemmilä, I. *J. Biomol. Screen.* **2002**, *7*, 223−231. (i) Préaudat, M.; Ouled-Diaf, J.; Alpha-Bazin, B.; Mathis, G.; Mitsugi, T.; Aono, Y.; Takahashi, K.; Takemoto, H. *J. Biomol. Screen.* **2002**, *7*, 267−274. (j) Lin, Z.; Wu, M.; Schäferling, M.; Wolfbeis, O. S. *Angew. Chem., Int. Ed.* **2004**, *43*, 1735−1738.

Scheme 1. (a) Schematic View of a Chromophore Incorporated into a Europium Emitter[a] and (b) the General Chromophore-to-Europium Ion Sensitization Process[b]

(a)

(b)

[a] The emission from Eu^{3+} after excitation of the chromophore is shown. [b] Light absorption and lowest-lying singlet excited state (S_1) formation at the sensitizing chromophore are followed by intersystem crossing (ISC), resulting in population of the lowest-lying triplet excited state (T_1). Subsequent chromophore-to-Eu^{3+} energy transfer leads to population of a metal-centered level, which deactivates from Eu^{3+}-emitting states to the relevant ground states.

the novel lanthanide complexes obtained showed a large enhancement of luminescence upon Zn^{2+} addition with an apparent dissociation constant K_d of 2.6 nM (295 K, pH 7.4).[19b] However, these compounds are unsuitable for biological applications, because of their short excitation wavelength, small emission enhancement, inconvenient pH sensitivity, insufficient selectivity for Zn^{2+}, etc. So, it is necessary to develop sensors with a longer excitation wavelength for biological applications without losing the high selectivity and high affinity for Zn^{2+}. Moreover, development of a simple sensor switch for Zn^{2+}, which would serve as both chromophore and Zn^{2+} receptor, would be useful. From this background, we set out to develop a novel lanthanide complex which can detect Zn^{2+} in biological systems, in the relevant concentration range.

Here we report the design and synthesis of the novel Zn^{2+}-sensitive luminescent lanthanide chemosensor [**Eu-7**]; upon complexation with Zn^{2+}, it exhibits strong, long-lived luminescence (of the order of milliseconds), and it also offers a large Stoke's shift (>250 nm), high water-solubility, and high selectivity for Zn^{2+} (Figure 1).

Results and Discussion

Design and Synthesis of [Eu-7] and [Gd-7]. N,N,N',N'-Tetrakis(2-pyridylmethyl)ethylenediamine[20] (TPEN) shows high selectivity for Zn^{2+} over other metal ions found under physiological conditions, such as Ca^{2+} and Mg^{2+}. Accordingly, we

(18) (a) Parker, D.; Dickins, R. S.; Puschmann, H.; Crossland, C.; Howard, J. A. K. *Chem. Rev.* **2002**, *102*, 1977−2010. (b) Quici, S.; Marzanni, G.; Carazzini, M.; Anelli, P. L.; Botta, M.; Gianolio, E.; Accorsi, G.; Armaroli, N.; Barigelletti, F. *Inorg. Chem.* **2002**, *41*, 2777−2784. (c) Latva, M.; Takalo, H.; Mukkala, V. M.; Matachescu, C.; Rodríguez-Ubis, J. C.; Kankare, J. *J. Lumin.* **1997**, *75*, 149−169. (d) Dadabhoy, A.; Faulkner, S.; Sammes, P. G. *J. Chem. Soc., Perkin Trans. 2* **2002**, 348−357.
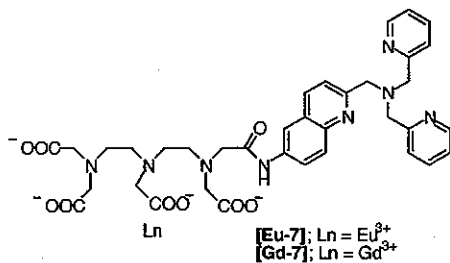
Figure 1. Structures of Eu^{3+} and Gd^{3+} N-{N-[2-N,N-bis(2-pyridylmethyl)-aminomethylquinolin-6-yl]carbamoylmethyl}-N,N',N'',N'''-diethylenetri-aminetetraacetic acid complexes: [Eu-7] and [Gd-7].

Figure 2. Time-delayed emission spectra (excitation at 320 nm) of [Eu-7] (50 μM) in the presence of various concentrations of Zn^{2+}: 0, 0.1, 0.2, 0.3, 0.4, 0.5, 0.6, 0.7, 0.8, 0.9, 1.0, 1.1, 1.2, 2.0, 3.0, 4.0, 5.0, and 10.0 equiv of Zn^{2+} with respect to [Eu-7]. These spectra were measured at pH 7.4 (100 mM HEPES buffer) and 22 °C using a delay time of 0.05 ms and a gate time of 1.00 ms. The inset shows the changes of the luminescence intensity at $\lambda = 614$ nm. The bands arise from $^5D_0 \rightarrow {}^7F_J$ transitions; the J values of the bands are labeled.

Figure 3. Absorbance spectra of 50 μM aqueous solution (100 mM HEPES buffer; pH 7.4) of [Eu-7] at 22 °C upon addition of aliquots of Zn^{2+}, which was added as $ZnSO_4$: 0, 0.2, 0.4, 0.6, 0.8, 1.0, 2.0, 3.0, 4.0, 5.0, and 10.0 equiv of Zn^{2+} with respect to [Eu-7]. The inset shows the spectra magnified between 290 and 360 nm.

designed a novel sensitive luminescent sensor for Zn^{2+} **[Eu-7]** by the combination of Eu^{3+}−diethylenetriaminepentaacetic acid (DTPA) complex and a quinoline-containing TPEN-based ligand for Zn^{2+}. The quinoline chromophore was selected as an antenna and a ligand, because quinoline has a longer excitation wavelength (>300 nm)[21] than pyridine and can coordinate to metal ions.

In the structure of **[Eu-7]**, the quinolyl chromophore is fixed close to the Eu^{3+} ion, allowing it to function as an antenna. The synthetic schemes for the lanthanide complexes, **[Eu-7]** and **[Gd-7]**, and details of the chemical characterization of compounds are provided in the Supporting Information.

Spectroscopic Characteristics of a Solution of [Eu-7] upon Addition of Zn^{2+}. The complex **[Eu-7]** in aqueous solution was characterized by a time-delayed luminescence spectrum with a delay time of 0.05 ms. The time-resolved luminescence emission intensity of **[Eu-7]** (50 μM) increased significantly (8.5-fold) upon addition of 1.0 equiv of Zn^{2+}, with a large Stoke's shift of >250 nm. The emission intensity remained at a plateau in the presence of an excess of Zn^{2+} (Figure 2). The luminescence emission displayed three bands at 579, 593, and 614 nm, corresponding to the deactivation from the $^5D_0$ excited state to $^7F_0$, $^7F_1$, and $^7F_2$ ground state, respectively.[18b,21b] The UV−vis absorption spectral change was monitored during Zn^{2+} addition. The absorption spectrum of **[Eu-7]** without Zn^{2+} had $\lambda_{max} = 249$ nm and broad bands at 330 and 318 nm, tailing out to 350 nm (Figure 3). The absorption spectrum of **[Eu-7]** changed upon addition of Zn^{2+} (0−1.0 equiv), with three isosbestic points at 334, 268, and 248 nm, and then remained at a plateau upon further addition of Zn^{2+} (Figure 3 and Figure S4), in accordance with the time-resolved luminescence spectra (Figure 2). The three peaks (330, 318, and 249 nm) of absorption changed to two peaks (320 and 253 nm) upon Zn^{2+} addition. The absorption wavelength changes between 300 and 350 nm were supposed to be due to the photophysical property change of the quinolyl moiety with Zn^{2+} chelation, whereas pyridine−Zn^{2+} coordination resulted in changes below 300 nm.[19b] Thus, 1:1 complex stoichiometry was observed in both the absorption and the luminescence emission spectra of **[Eu-7]**. The Job's plot using the luminescence emission intensity of Eu^{3+} at 614
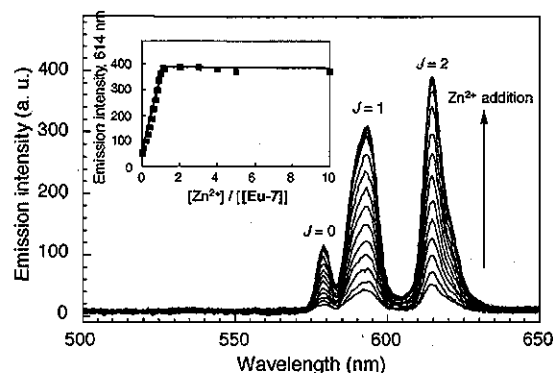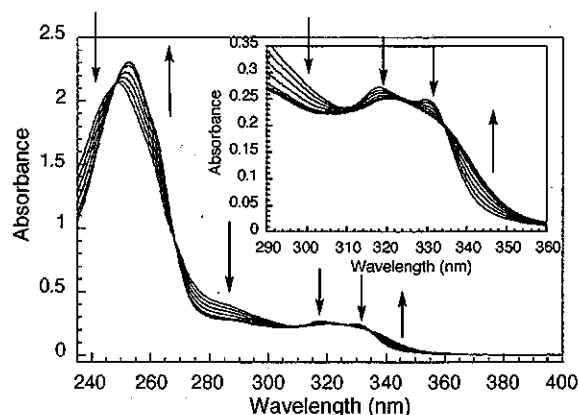
nm for the complex of **[Eu-7]** and Zn^{2+} also indicated the presence of the 1:1 complex (see Supporting Information).[22] For **[Eu-7]** (20 μM), the fluorescence emission spectra were measured without a delay time, with excitation at 320 nm (Figure 4). In the fluorescence emission of **[Eu-7]**, one band with a short lifetime appeared at 397 nm with a concomitant linear fluorescence increase following addition of Zn^{2+} at between 0 and 1.0 equiv to **[Eu-7]**, and it remained at a plateau with further Zn^{2+} addition (Figure S6). The short-lived fluorescence at 397 nm can be ascribed to direct emission from the quinolyl moiety of **[Eu-7]**.[21a,b] All these results can be rationalized in terms of 1:1 complex formation of **[Eu-7]** with Zn^{2+}, via the quinolyl ligand.

Luminescence and Chemical Properties of [Eu-7] and [Gd-7]. The luminescence and chemical properties of **[Eu-7]** and **[Gd-7]** are listed in Table 1. **[Eu-7]** and **[Gd-7]**, even at 10 mM, were highly water-soluble. The phosphorescence spectra of **[Gd-7]** were measured in MeOH:EtOH = 1:1 at 77 K in the absence and in the presence of Zn^{2+}. The triplet energy levels for free and Zn^{2+}-bound **[Gd-7]** were around 20 790 and 20 576

(19) (a) Reany, O.; Gunnlaugsson, T.; Parker, D. J. Chem. Soc., Perkin Trans. 2 2000, 1819−1831. (b) Hanaoka, K.; Kikuchi, K.; Kojima, H.; Urano, Y.; Nagano, T. Angew. Chem., Int. Ed. 2003, 42, 2996−2999. (c) Reany, O.; Gunnlaugsson, T.; Parker, D. Chem. Commun. 2000, 473−474.

(20) Sillén, L. G.; Martell, A. E. Stability Constants of Metal-Ion Complexes; Special Publication No. 17; The Chemical Society: Burlington House, London, 1964.

(21) (a) Gunnlaugsson, T. Tetrahedron Lett. 2001, 42, 8901−8905. (b) Gunnlaugsson, T.; MacDónaill, D. A.; Parker, D. J. Am. Chem. Soc. 2001, 123, 12866−12876. (c) Manning, H. C.; Goebel, T.; Marx, J. N.; Bornhop, D. J. Org. Lett. 2002, 4, 1075−1078. (d) Jotterand, N.; Pearce, D. A.; Imperiali, B. J. Org. Chem. 2001, 66, 3224−3228.

(22) Nabeshima, T.; Tsukada, N.; Nishijima, K.; Ohshiro, H.; Yano, Y. J. Org. Chem. 1996, 61, 4342−4350.
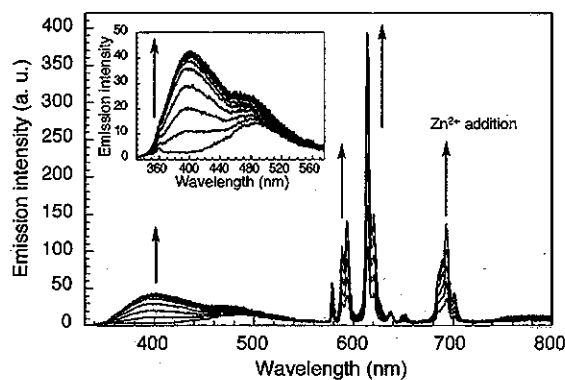
Figure 4. Fluorescence spectra of [Eu-7] (20 μM) in 100 mM HEPES buffer at pH 7.4 without a delay time upon the addition of increasing amounts of Zn²⁺: 0, 0.2, 0.4, 0.6, 0.8, 1.0, 2.0, 3.0, 4.0, 5.0, and 10.0 equiv of Zn²⁺ with respect to [Eu-7]. Excitation at 320 nm, 22 °C. The inset shows the spectra magnified between 330 and 575 nm.

Table 1. Luminescence and Chemical Properties

	apparent K_d for Zn²⁺ (nM)[a]	ϕ (%)[b] Zn²⁺ free	ϕ (%)[b] Zn²⁺ complex	τ_{H_2O} (ms)[c] Zn²⁺ free	τ_{H_2O} (ms)[c] Zn²⁺ complex	τ_{D_2O} (ms)[d] Zn²⁺ free	τ_{D_2O} (ms)[d] Zn²⁺ compex	q^e Zn²⁺ free	q^e Zn²⁺ complex
[Eu-7]	59	0.9	7.4	0.52	0.58	2.03	2.23	1.42	1.22

	triplet state energy (cm⁻¹)[f] free	triplet state energy (cm⁻¹)[f] Zn²⁺ complex	r_1 (mM⁻¹ s⁻¹)[g] free	r_1 (mM⁻¹ s⁻¹)[g] Zn²⁺ complex
[Gd-7]	20790	20576	6.05	5.81

[a] [Zn²⁺] was controlled by using Zn²⁺/NTA systems below 398 nM free Zn²⁺ and unbuffered Zn²⁺ above 200 μM free Zn²⁺. The buffer contained 100 mM HEPES, pH 7.4, *I* = 0.1 (NaNO₃). [b] Quantum yields were calculated using [Ru(bipy)₃]Cl₂ (bipy = 2,2′-bipyridine; ϕ = 0.028 in water) as a standard, and measured in 100 mM HEPES buffer at pH 7.4, 25 °C. [c] In H₂O-based buffer (100 mM HEPES buffer; pH 7.4). [d] In D₂O-based buffer (100 mM HEPES buffer; pD 7.4). [e] q values were estimated using the equation $q^{Eu} = 1.2(\tau_{H_2O}^{-1} - \tau_{D_2O}^{-1} - 0.25)$, which allows for the contribution of unbound water molecules.[23] [f] In MeOH:EtOH = 1:1 at 77 K. [g] The R_1 relaxivity as measured at 20 MHz and 25 °C in 100 mM HEPES buffer (pH 7.4).

cm⁻¹, respectively, and both were sufficiently close to the ⁵D₀ level, the excited state, of Eu³⁺ (E = 17 250 cm⁻¹).[23] The luminescence quantum yield (ϕ) was 0.9% before addition of Zn²⁺ and was increased 8.2-fold to 7.4% by Zn²⁺ addition, under air-equilibrated conditions. This luminescence quantum yield is sufficiently large for luminescence detection. Further, the binding affinity for Zn²⁺ was assessed by using the luminescence intensity. The affinity of [Eu-7] for Zn²⁺ ions was measured at pH 7.4, 22 °C, in a high salt background (100 mM HEPES buffer, *I* = 0.1 (NaNO₃)). The apparent dissociation constant K_d for Zn²⁺ was calculated to be 59 nM. This K_d value for Zn²⁺ was larger than that reported for tris(2-pyridylmethyl)-amine (TPA) (K_d = 0.014 nM; pH = 7.4, 298 K, *I* = 0.1),[24] probably due to a larger steric repulsion in the case of the quinolyl substituent than the pyridyl substituent, but the value is still sufficiently small for biological applications.[25] Measurements of the decay rate constants of the Eu³⁺ excited state were carried out in both H₂O and D₂O, in the absence and in the

presence of Zn²⁺ (see Supporting Information). The luminescence lifetimes of [Eu-7] were found to be 0.52 (without Zn²⁺) and 0.58 (with Zn²⁺) ms in H₂O (τ_{H_2O}), and 2.03 (without Zn²⁺) and 2.23 (with Zn²⁺) ms in D₂O (τ_{D_2O}). These values indicated that the numbers of coordinated water molecules (q values) at the metal center were 1.42 and 1.22, respectively, according to eq 1.[26] Thus, the lanthanide hydration state was hardly affected

no. of water molecules:

$$q^{Eu} = 1.2(\tau_{H_2O}^{-1} - \tau_{D_2O}^{-1} - 0.25) \quad (1)$$

by the addition of Zn²⁺. Therefore, it can be considered that the increase of the emission intensity caused by Zn²⁺ addition was not due to a change in the direct interaction of water molecules with Eu³⁺.

Next, the spatial arrangement of [Eu-7] was further assessed by measuring the relaxometric properties. The water proton relaxivity R_1 of Gd³⁺ complexes is routinely used as an important parameter for MRI contrast agents.[27] The relaxation enhancement is modulated by the electron−nucleus dipolar interaction, which can be changed by rotation of the complex, by electron spin relaxation of the metal ion, and by the co-ordinated exchange of water molecules.[28] The R_1 relaxivity of [Gd-7] at 20 MHz showed similar values in the absence and in the presence of Zn²⁺, i.e., 6.05 and 5.81 mM⁻¹ s⁻¹, respectively. This result indicates that the environment around the Eu³⁺ ion of [Eu-7] was hardly changed by Zn²⁺ binding.

Effect of pH and Other Cations on the Long-Lived Luminescence Intensity. The luminescence emission intensity of [Eu-7] at 614 nm was examined at various pH values, with excitation at 320 nm. There was almost no effect of H⁺ on the emission spectrum of [Eu-7] between pH 3.6 and 8.8 either in the presence or in the absence of Zn²⁺ (see Supporting Information). Thus, the luminescence emission intensity of [Eu-7] is stable at around physiological pH. Parker et al. reported a Zn²⁺-sensitive luminescent lanthanide probe based on photo-induced electron transfer (PeT) from the benzylic nitrogen to the chromophore's singlet excited state.[19a,c] This approach has the disadvantage that the pivotal nitrogen for Zn²⁺ binding can also be protonated at lower pH, resulting in strong luminescence owing to inhibition of PeT. However, our compound [Eu-7] was not affected by lowering of the pH. The tertiary amine of [Eu-7] can be protonated at around pH 3.6, because TPA has pK_a values of 6.10, 4.28, and 2.49.[24] Thus, the finding of insensitivity to lower pH means that the luminescence augmentation was not due to cessation of PeT from tertiary amine. We think that this pH stability of the luminescence is one of the key advantages of [Eu-7].

The effect of adding Na⁺, K⁺, Ca²⁺, Mg²⁺, and various heavy metal ions on the luminescence emission intensity of [Eu-7] was also examined. Luminescence emission enhancement of

(23) (a) Crosby, G. A.; Whan, R. E.; Alire, R. M. *J. Chem. Phys.* **1961**, *34*, 743−748. (b) Stein, G.; Würzberg, E. *J. Chem. Phys.* **1975**, *62*, 208−213.
(24) Martell, A. E.; Smith, R. M. *NIST Critically Selected Stability Constants of Metal Complexes*; NIST Standard Reference Database 46, Version 6.0; NIST: Gaithersburg, MD, 2001.
(25) (a) Weiss, J. H.; Sensi, S. L.; Koh, J. Y. *Trends Pharmacol. Sci.* **2000**, *21*, 395−401. (b) Li, Y.; Hough, C. J.; Suh, S. W.; Sarvey, J. M.; Frederickson, C. J. *J. Neurophysiol.* **2001**, *86*, 2597−2604. (c) Li, Y.; Hough, C. J.; Frederickson, C. J.; Sarvey, J. M. *J. Neurosci.* **2001**, *21*, 8015−8025.

(26) Beeby, A.; Clarkson, I. M.; Dickins, R. S.; Faulkner, S.; Parker, D.; Royle, L.; de Sousa, A. S.; Williams, J. A. G.; Woods, M. *J. Chem. Soc., Perkin Trans. 2* **1999**, 493−503.
(27) (a) Caravan, P.; Ellison, J. J.; McMurry, T. J.; Lauffer, R. B. *Chem. Rev.* **1999**, *99*, 2293−2352. (b) Lowe, M. P. *Aust. J. Chem.* **2002**, *55*, 551−556. (c) Li, W. H.; Fraser, S. E.; Meade, T. J. *J. Am. Chem. Soc.* **1999**, *121*, 1413−1414. (d) Li, W. H.; Parigi, G.; Fragai, M.; Luchinat, C.; Meade, T. J. *Inorg. Chem.* **2002**, *41*, 4018−4024. (e) Moats, R. A.; Fraser, S. E.; Meade, T. J. *Angew. Chem., Int. Ed. Engl.* **1997**, *36*, 726−728. (f) Louie, A. Y.; Hüber, M. M.; Ahrens, E. T.; Rothbächer, U.; Moats, R.; Jacobs, R. E.; Fraser, S. E.; Meade, T. J. *Nat. Biotechnol.* **2000**, *18*, 321−325.
(28) Merbach, A. E.; Tóth, É. *The Chemistry of Contrast Agents in Medical Magnetic Resonance Imaging*; John Wiley & Sons, Ltd.: Chichester, 2001.